Supplementary Information

Designing negative feedback loops in enzymatic coacervate droplets

Nisha Modi[1], Siwei Chen[1], Imelda N. A. Adjei[2], Briana L. Franco[1], Kyle J. M. Bishop[*1], and Allie C. Obermeyer[†1]

[1]Department of Chemical Engineering, Columbia University, New York, NY, USA
[2]Department of Biomedical Engineering, Columbia University, New York, NY, USA

Contents

*kyle.bishop@columbia.edu

†aco2134@columbia.edu

1 Model of enzymatic pH change in solution

1.1 Reactions

We consider the following reactions that describe the acid-base dissociation of water and hydrogen peroxide and the catalytic decomposition of peroxide by a pseudo-first-order reaction

$$H_2O \underset{k_w^-}{\overset{k_w^+}{\rightleftharpoons}} H^+ + OH^- \tag{S1}$$

$$H_2O_2 \underset{k_p^-}{\overset{k_p^+}{\rightleftharpoons}} H^+ + HO_2^- \tag{S2}$$

$$H_2O_2 \xrightarrow[\text{catalase}]{k_{obs}} H_2O + \tfrac{1}{2}O_2 \tag{S3}$$

Assuming dilute solutions and mass action kinetics, the corresponding reaction rates are modeled as

$$R_w = k_w^- \left(K_w - C_{H^+} C_{OH^-} \right) \tag{S4}$$

$$R_p = k_p^- \left(K_p C_{H_2O_2} - C_{H^+} C_{HO_2^-} \right) \tag{S5}$$

$$R_{cat} = k_{obs} C_{H_2O_2} \tag{S6}$$

where $K_w = 10^{-14}$ M^2 is the self-ionization constant of water (at 25 °C and zero ionic strength), and $K_p = k_p^+/k_p^- = 2.399 \times 10^{-12}$ M is the dissociation constant of hydrogen peroxide (based on the reported pK_a of 11.62).

As shown below, the rate of pH increase is controlled by the enzyme kinetics, which may depend on changes in the pH and the peroxide concentration.[1] For simplicity, we neglect these complicating factors and adopt a first-order rate law (S3) for the enzymatic decomposition of peroxide. This simplification does not alter the predicted magnitude of the pH increase, which is controlled by the acid-base equilibria in the limit of complete peroxide decomposition. Moreover, the first-order dependence on $C_{H_2O_2}$ is consistent with the reported Michaelis-Menten kinetics when the peroxide concentration is much lower than the Michaelis constant—that is, when $C_{H_2O_2} \ll K_M = 1.1$ M as in our experiments.[1] Studies of catalase kinetics[2] have further shown that the observed rate constant k_{obs} is linearly proportional to the enzyme concentration as

$$k_{obs} = k_s E_o \tag{S7}$$

where E_o is the molar enzyme concentration, and k_s is a second order rate constant—often expressed as k_{cat}/K_m in the context of Michaelis-Menten kinetics.[1]

1.2 Initial equilibrium concentrations

In the absence of catalytic decomposition ($k_{obs} = 0$), the species concentrations approach stable equilibrium values governed by

$$K_w = C_{H^+}^{eq} C_{OH^-}^{eq} \quad \text{and} \quad K_p = \frac{C_{H^+}^{eq} C_{HO_2^-}^{eq}}{C_{H_2O_2}^{eq}} \tag{S8}$$

Additionally, the total concentration of peroxide is constant such that

$$C_{\mathrm{p}} = C_{\mathrm{H_2O_2}}^{\mathrm{eq}} + C_{\mathrm{HO_2^-}}^{\mathrm{eq}} \tag{S9}$$

If the solution pH and the total peroxide concentration C_{p} are specified, the above equations can be solved to obtain the following equilibrium concentrations

$$C_{\mathrm{H_2O_2}}^{\mathrm{eq}} = \frac{C_{\mathrm{H^+}}^{\mathrm{eq}} C_{\mathrm{p}}}{C_{\mathrm{H^+}}^{\mathrm{eq}} + K_{\mathrm{p}}}, \quad C_{\mathrm{HO_2^-}}^{\mathrm{eq}} = \frac{K_{\mathrm{p}} C_{\mathrm{p}}}{C_{\mathrm{H^+}}^{\mathrm{eq}} + K_{\mathrm{p}}}, \quad C_{\mathrm{OH^-}}^{\mathrm{eq}} = \frac{K_{\mathrm{w}}}{C_{\mathrm{H^+}}^{\mathrm{eq}}} \tag{S10}$$

where $C_{\mathrm{H^+}}^{\mathrm{eq}} = 10^{-\mathrm{pH}}$ is the specified $\mathrm{H^+}$ concentration.

1.3 Final asymptotic concentrations

The addition of catalase to an equilibrated solution of hydrogen peroxide causes its catalytic decomposition thereby consuming all $\mathrm{H_2O_2}$ and $\mathrm{HO_2^-}$ present in the solution

$$C_{\mathrm{H_2O_2}}^{\infty} = 0 = C_{\mathrm{H_2O_2}}^{\mathrm{eq}} - \xi_{\mathrm{p}}^{\infty} - \xi_{\mathrm{cat}}^{\infty} \tag{S11}$$

$$C_{\mathrm{HO_2^-}}^{\infty} = 0 = C_{\mathrm{HO_2^-}}^{\mathrm{eq}} + \xi_{\mathrm{p}}^{\infty} \tag{S12}$$

where $\xi_{\mathrm{p}}^{\infty}$ and $\xi_{\mathrm{cat}}^{\infty}$ are the extent of reactions (S2) and (S3) in the limit of long time ($t \to \infty$). Similarly, the asymptotic concentrations of $\mathrm{H^+}$ and $\mathrm{OH^-}$ are given by

$$C_{\mathrm{H^+}}^{\infty} = C_{\mathrm{H^+}}^{\mathrm{eq}} + \xi_{\mathrm{w}}^{\infty} + \xi_{\mathrm{p}}^{\infty} \tag{S13}$$

$$C_{\mathrm{OH^-}}^{\infty} = C_{\mathrm{OH^-}}^{\mathrm{eq}} + \xi_{\mathrm{w}}^{\infty} \tag{S14}$$

where $\xi_{\mathrm{w}}^{\infty}$ is the limiting extent of reaction (S1). These asymptotic concentrations must also satisfy the equilibrium relation for water dissociation—namely, $K_{\mathrm{w}} = C_{\mathrm{H^+}}^{\infty} C_{\mathrm{OH^-}}^{\infty}$. We can therefore solve for the unknown reaction extents $\xi_{\mathrm{w}}^{\infty}$ and $\xi_{\mathrm{p}}^{\infty}$ to determine the final $\mathrm{H^+}$ concentration relative to the initial concentration

$$\frac{C_{\mathrm{H^+}}^{\infty}}{C_{\mathrm{H^+}}^{\mathrm{eq}}} = \frac{1}{2}\left(1 - \frac{K_{\mathrm{w}}}{H^2} - \frac{C_{\mathrm{p}}K_{\mathrm{p}}}{H(H+K_{\mathrm{p}})} + \sqrt{\left(1 + \frac{K_{\mathrm{w}}}{H^2} - \frac{K_{\mathrm{p}}C_{\mathrm{p}}}{H(H+K_{\mathrm{p}})}\right)^2 + 4\frac{K_{\mathrm{w}}}{H^2}\frac{K_{\mathrm{p}}C_{\mathrm{p}}}{H(H+K_{\mathrm{p}})}}\right) \tag{S15}$$

On the right hand side, we abbreviate the initial $\mathrm{H^+}$ concentration as $C_{\mathrm{H^+}}^{\mathrm{eq}} \to H$ for brevity. The pH increase is related to the logarithm of this ratio as $\Delta\mathrm{pH} = \log_{10}(C_{\mathrm{H^+}}^{\mathrm{eq}}/C_{\mathrm{H^+}}^{\infty})$ (see Fig. S1a). For the experimental conditions (i.e., $K_{\mathrm{w}}/C_{\mathrm{p}} \ll K_{\mathrm{p}} \ll \sqrt{K_{\mathrm{p}}C_{\mathrm{p}}}$), we identify the following approximations for the pH increase as a function of the initial pH

$$\frac{C_{\mathrm{H^+}}^{\infty}}{C_{\mathrm{H^+}}^{\mathrm{eq}}} \approx \begin{cases} 1 - \frac{K_{\mathrm{p}}C_{\mathrm{p}}}{H^2} & \text{for} \quad \sqrt{K_{\mathrm{p}}C_{\mathrm{p}}} \ll H \\[2mm] \frac{K_{\mathrm{w}}}{K_{\mathrm{w}}+K_{\mathrm{p}}C_{\mathrm{p}}} & \text{for} \quad K_{\mathrm{p}} \ll H \ll \sqrt{K_{\mathrm{p}}C_{\mathrm{p}}} \\[2mm] \frac{\sqrt{4K_{\mathrm{w}}+C_{\mathrm{p}}^2}-C_{\mathrm{p}}}{2H} & \text{for} \quad K_{\mathrm{w}}/C_{\mathrm{p}} \ll H \ll \sqrt{K_{\mathrm{p}}C_{\mathrm{p}}} \\[2mm] 1 - \frac{C_{\mathrm{p}}H}{K_{\mathrm{w}}} & \text{for} \quad H \ll K_{\mathrm{w}}/C_{p} \end{cases} \tag{S16}$$

4

The largest pH increase is achieved in the region II and increases monotonically with increasing peroxide concentration as

$$\Delta\text{pH} \approx \log_{10}\left(1 + \frac{K_\text{p}C_\text{p}}{K_\text{w}}\right) \tag{S17}$$

for $K_\text{p} \ll H \ll \sqrt{K_\text{p}/C_\text{p}}$. Figure S1b shows this approximation along with the exact result of equation (S15).

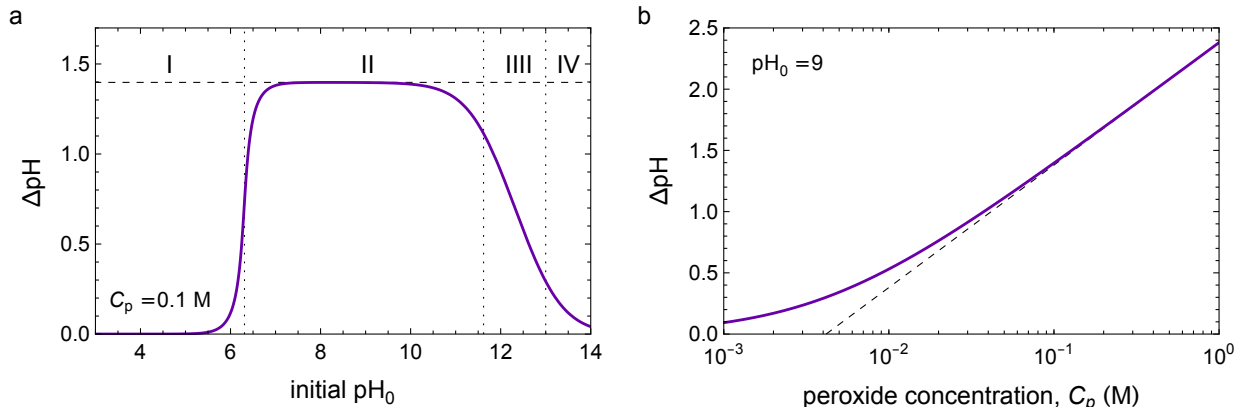**Figure S1:** (a) pH increase predicted by equation (S15) as a function of the initial pH_0 for a total peroxide concentration of $C_\text{p} = 0.1$ M. Vertical dotted lines show the concentrations, $\sqrt{K_\text{p}C_\text{p}} \gg K_\text{p} \gg K_\text{w}/C_\text{p}$ (left to right), that separate the four regions summarized by equation (S16). The horizontal dashed line shows the approximate result of equation (S17) for region II. (b) Predicted pH increase as a function of the peroxide concentration C_p for an initial $\text{pH}_0 = 9$ (region II). The dashed line shows the asymptotic result $\Delta\text{pH} = \log_{10}(K_\text{p}C_\text{p}/K_\text{w})$. Other parameter values are $K_\text{w} = 10^{-14}$ M^2 and $K_\text{p} = 2.399 \times 10^{-12}$ M.

1.4 Effect of added buffer

The final concentration of Tris in the reaction solution is 8 μM in experiments carried out to characterise the reaction-induced pH change as a function of initial solution pH (see Fig. 2a) and initial H_2O_2 concentration (see Fig. 2b). Near neutral pH, the presence of even small amounts of buffer can alter the reaction-induced pH increase predicted by the model above. To account for these effects, we introduce an additional acid-dissociation reaction

$$\text{HA}^+ \underset{k_\text{a}^-}{\overset{k_\text{a}^+}{\rightleftharpoons}} \text{H}^+ + \text{A} \tag{S18}$$

where A denotes an added base such as Tris (i.e., tris(hydroxymethyl)aminomethane), and HA^+ denotes its conjugate acid. The dissociation constant for this reaction is denoted $K_\text{a} = k_\text{a}^+/k_\text{a}^-$, which is $K_\text{a} = 8.51 \times 10^{-9}$ M for Tris (based on a reported pK_a of 8.07 at 25 °C). Together with reactions (S1) and (S2), reaction (S18) describes the acid-base equilibrium for water, peroxide, and the added base. The equilibrium concentrations of all species before and after consumption of H_2O_2 are computed numerically as described above for the simpler case without added buffer.

1.5 Transient concentrations

Finally, we consider the speed at which the pH increase occurs. The extents of the three reactions (S1)–(S3) evolve in time as

$$\dot{\xi}_{\mathrm{w}} = r_{\mathrm{w}} = k_{\mathrm{w}}^- \left(K_{\mathrm{w}} - (C_{\mathrm{H^+}}^{\mathrm{eq}} + \xi_{\mathrm{w}} + \xi_{\mathrm{p}})(C_{\mathrm{OH^-}}^{\mathrm{eq}} + \xi_{\mathrm{w}}) \right) \tag{S19}$$

$$\dot{\xi}_{\mathrm{p}} = r_{\mathrm{p}} = k_{\mathrm{p}}^- \left(K_{\mathrm{p}}(C_{\mathrm{H_2O_2}}^{\mathrm{eq}} - \xi_{\mathrm{p}} - \xi_{\mathrm{cat}}) - (C_{\mathrm{H^+}}^{\mathrm{eq}} + \xi_{\mathrm{w}} + \xi_{\mathrm{p}})(C_{\mathrm{HO_2^-}}^{\mathrm{eq}} + \xi_{\mathrm{p}}) \right) \tag{S20}$$

$$\dot{\xi}_{\mathrm{cat}} = r_{\mathrm{cat}} = k_{\mathrm{obs}}(C_{\mathrm{H_2O_2}}^{\mathrm{eq}} - \xi_{\mathrm{p}} - \xi_{\mathrm{cat}}) \tag{S21}$$

with initial conditions $\xi_{\mathrm{w}} = \xi_{\mathrm{p}} = \xi_{\mathrm{cat}} = 0$ at time $t = 0$. Here, we have expressed the relevant species concentrations $C_{\mathrm{H^+}}$, $C_{\mathrm{OH^-}}$, $C_{\mathrm{H_2O_2}}$, $C_{\mathrm{HO_2^-}}$ in terms of their initial (equilibrium) values and the reaction extents. At time zero, the acid-base reactions (S1) and (S2) are assumed to be at equilibrium such that

$$r_{\mathrm{w}} = r_{\mathrm{p}} = 0 \quad \text{at} \quad t = 0 \tag{S22}$$

Given the initial pH_0 and the total peroxide concentration C_{p}, the initial equilibrium concentrations are given by equation (S10). The rate constants k_{w}^- and k_{p}^- for ion association are assumed to be diffusion limited with a common value equal of 1.4×10^{11} $\mathrm{M^{-1}s^{-1}}$ as reported for water.[3] With these assumptions, equations (S19)–(S21) can be integrated numerically to determine the transient species concentrations. Figure S2 shows the transient pH for the experimentally relevant conditions of $k_{\mathrm{obs}} = 0.1$ $\mathrm{s^{-1}}$, $C_{\mathrm{p}} = 0.1$ M, and $\mathrm{pH}_0 = 9$.
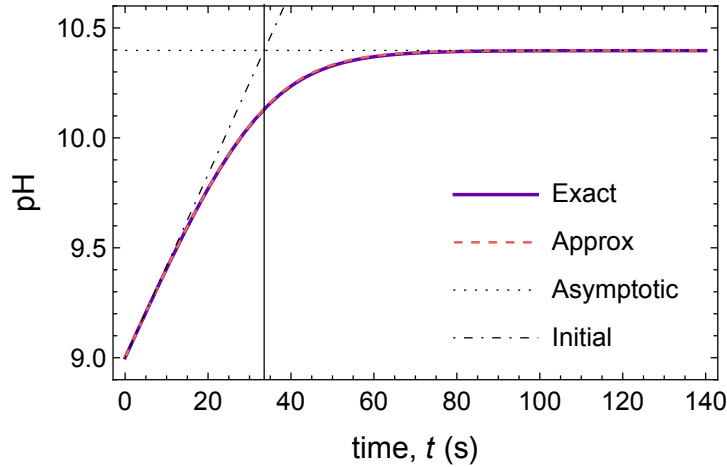
t*

Figure S2: Predicted pH as a function of time for the catalytic decomposition of $C_{\mathrm{p}} = 0.1$ M hydrogen peroxide with an initial $\mathrm{pH}_0 = 9$. The solid curve denotes the "exact" solution obtained by numerical integration of equations (S19)–(S21). The dashed curve is the approximate solution of equation (S26); the dotted curve is the asymptotic result. The vertical line represents the characteristic time scale of equation (S27).

Under the experimental conditions, useful approximate solutions can be derived by assuming that acid-base equilibration is fast relative to peroxide decomposition. At low pH values (pH <

11.62), nearly all peroxide is protonated (i.e., $C_{H_2O_2}^{eq} \approx C_p$), and the acid-base equilibria can be accurately approximated as

$$K_w = (C_{H^+}^{eq} + \xi_w + \xi_p)(C_{H^+}^{eq}/K_w + \xi_w) \quad \text{and} \quad K_p \approx \frac{(C_{H^+}^{eq} + \xi_w + \xi_p)(K_pC_p/C_{H^+}^{eq} + \xi_p)}{(C_p - \xi_{cat})} \quad \text{(S23)}$$

Solving these equations for the reaction extents ξ_w amd ξ_p, one can express the H^+ concentration in terms of the initial concentrations of peroxide and H^+ and the extent of peroxide decomposition

$$C_{H^+} = C_{H^+}^{eq}\left(1 - \frac{K_p\xi_{cat}}{K_w + K_pC_p}\right) + O(C_{H^+}^{eq\;3}) \quad \text{(S24)}$$

where higher order terms are negligible for $C_{H^+}^{eq} \ll K_p$. Thus, there is a linear relationship between the H^+ concentration and the extent of peroxide decomposition, which is well approximated as

$$\dot{\xi}_{cat} \approx k_{obs}(C_p - \xi_{cat}) \quad \text{(S25)}$$

Integrating equation (S25) and substituting into equation (S24), the "exact" numerical solution for the transient pH is well approximated as

$$pH(t) \approx pH_0 - \log_{10}\left(\frac{K_w + K_pC_pe^{-k_{obs}t}}{K_w + K_pC_p}\right) \quad \text{(S26)}$$

Figure S2 shows that this expression provides an excellent approximation for the pH response under conditions relevant to the experiments.

The characteristic time scale t^* for the pH change to occur can be estimated by the geometric construction illustrated in Figure S2. The linearized pH increase at early times intersects the asymptotic pH at

$$t^* = \frac{K_pC_p + K_w}{k_{obs}K_pC_p}\ln\left(1 + \frac{K_pC_p}{K_w}\right) = \frac{1}{k_{obs}}\frac{\ln(10)10^{\Delta pH}\Delta pH}{(10^{\Delta pH} - 1)} \quad \text{(S27)}$$

Other Rate Laws

As noted above, the first-order rate law (S6) for peroxide decomposition was selected for its simplicity; however, it is possible to use other rate laws as needed to describe the dependence on peroxide concentration and/or pH. For example, the common Michaelis-Menten rate law for enzyme kinetics implies that

$$\dot{C}_{H_2O_2} = \frac{V_{max}C_{H_2O_2}}{K_M + C_{H_2O_2}} \quad \text{(S28)}$$

where V_{max} is the maximum rate, and K_M is the Michaelis constant for substrate-enzyme dissociation. Integrating equation (S28) and substituting into equation (S24), the transient pH is well approximated as

$$pH(t) \approx pH_0 - \log_{10}\left(\frac{K_w + K_pK_M \text{ ProductLog}\left(\frac{C_p}{K_M}e^{(C_p - V_{max}t)/K_M}\right)}{K_w + K_pC_p}\right) \quad \text{(S29)}$$

where ProductLog( ) denotes the Lambert W function.

2 Model of enzymatic pH change in a spherical drop

To describe the transient pH changes in and around a spherical drop enriched with catalase, we consider a simple reaction-diffusion model in which peroxide is decomposed at different rates, $k_{\mathrm{obs}}^{\mathrm{in}}$ and $k_{\mathrm{obs}}^{\mathrm{out}}$, inside and outside of the drop. As these rate constants are proportional to the enzyme concentration, peroxide is decomposed at a faster rate inside of the drop than outside resulting in concentration gradients that drive the diffusive delivery of $\mathrm{H_2O_2}$ from the solution. Similarly, the $\mathrm{OH^-}$ concentration inside the drop rises faster than that outside the drop resulting in pH differences driven by the enzymatic reaction. Importantly, these reaction-induced concentration differences depend on the drop radius a with larger drops supporting larger concentration differences.

In the model, the concentrations C_i^{in} of species $i = \{\mathrm{H_2O_2}, \mathrm{HO_2}^-, \mathrm{H^+}, \mathrm{OH^-}\}$ inside the drop ($0 \leq r \leq a$) are governed by reaction-diffusion equations of the form

$$\frac{\partial C_i^{\mathrm{in}}}{\partial t} = \frac{D_i}{r^2} \frac{\partial}{\partial r} \left(r^2 \frac{\partial C_i^{\mathrm{in}}}{\partial r} \right) + \sum_j \nu_{ij} R_j^{\mathrm{in}} \tag{S30}$$

where D_i is the species diffusivity, ν_{ij} is the stoichiometric coefficient for species i in reaction j, and R_j^{in} is the reaction rate inside the drop. We consider reactions (S1)—(S3) describing the acid-base equilibrium of peroxide and its enzymatic decomposition as detailed in the previous section. Diffusion coefficients are approximated by their limiting values in dilute aqueous solutions. Reaction rate constants are assumed to be the same inside ($r < a$) and outside ($r > a$) of the drop with the exception of $k_{\mathrm{obs}}^{\mathrm{in}} > k_{\mathrm{obs}}^{\mathrm{out}}$. These simplifying assumptions neglect the possibility that species diffusion is slower in the condensed phase or that reaction rate constants are altered by the drop environment.

Outside the coacervate droplets, the species concentrations in the well-mixed solution are assumed to be spatially uniform and evolve in time as

$$\frac{dC_i^{\mathrm{out}}}{dt} = \sum_j \nu_{ij} R_j^{\mathrm{out}} - \frac{AD_i}{V} \left. \frac{\partial C_i^{\mathrm{in}}}{\partial r} \right|_{r=a} \tag{S31}$$

Here, the first term describes the effects of reactions in solution, while the second describes the diffusive exchange of species with the droplet. The ratio between the droplet surface area A and the solution volume V (per droplet) is related to the droplet volume fraction ϕ and radius a as $A/V = 3\phi/a(1-\phi)$. At the surface of the droplet ($r = a$), the species concentration is assumed to be continuous such that

$$C_i^{\mathrm{in}}(a, t) = C_i^{\mathrm{out}}(t) \tag{S32}$$

This simplifying assumption neglects the possible enrichment of ionic species within the coacervate phase.

Initially, the $\mathrm{H^+}$ and $\mathrm{OH^-}$ concentrations are spatially uniform inside and outside of the drop corresponding to a common $\mathrm{pH_0}$ thoughout the system

$$C_{\mathrm{H^+}}^{\mathrm{in}}(r, 0) = C_{\mathrm{H^+}}^{\mathrm{out}}(0) = H_0 \tag{S33}$$

$$C_{\mathrm{OH^-}}^{\mathrm{in}}(r, 0) = C_{\mathrm{OH^-}}^{\mathrm{out}}(0) = \frac{K_{\mathrm{w}}}{H_0} \tag{S34}$$

where $H_0 = 10^{-\text{pH}_0}$. As in our experiments, hydrogen peroxide is initially present only outside of the drop such that

$$C_{\text{H}_2\text{O}_2}^{\text{in}}(r,0) = 0 \quad \text{and} \quad C_{\text{H}_2\text{O}_2}^{\text{out}}(0) = \frac{H_0 C_\text{p}}{H_0 + K_\text{p}} \frac{1}{1-\phi} \tag{S35}$$

$$C_{\text{HO}_2^-}^{\text{in}}(r,0) = 0 \quad \text{and} \quad C_{\text{HO}_2^-}^{\text{out}}(0) = \frac{K_\text{p} C_\text{p}}{H_0 + K_\text{p}} \frac{1}{1-\phi} \tag{S36}$$

where C_p is the nominal peroxide concentration averaged over the total system volume, and ϕ is the volume fraction of the drop phase. In this closed system, the concentration profiles evolve in time to a new uniform state, in which all peroxide is consumed. We first consider the transient concentration profiles that accompany the reaction-induced pH increase. We then consider an open system in which the supply of chemical fuel(s) enable the formation of non-uniform pH gradients at steady-state.

2.1 Transient pH increase

Figure S3 shows results of the reaction-diffusion model for droplets of different sizes. The model parameters correspond to the experiments in Figure 5 of the main text. Based on the measured reaction time $t^* = 6.6$ s for the decomposition of 100 mM H_2O_2 by 0.22 mg/mL catalase at pH 9 (see Table SII), we assume an average rate constant $k_{\text{obs}} = 0.51$ s^{-1} consistent with equation (S27). We further assume that the rate of peroxide decomposition is proportional to the local catalase concentration such that rate constants inside and outside the drop are approximated as

$$k_{\text{obs}}^{\text{in}} = \frac{1-f}{\phi} k_{\text{obs}} \quad \text{and} \quad k_{\text{obs}}^{\text{out}} = \frac{f}{1-\phi} k_{\text{obs}} \tag{S37}$$

where $f = 0.47$ is the fraction of catalase in the dilute phase outside of the drop (see Fig. 3c).[1] The fraction ϕ of the condensed phase is not known precisely but is estimated to be $\phi \approx 0.001$.[4–6] With these parameter estimates, we solve the reaction-diffusion equations numerically using a commercial finite element solver (COMSOL v5.5).

Figure S3a shows the transient pH in solution as a function of time for catalase droplets of different sizes spanning $a = 0.1 - 1000$ μm. These results are accurately reproduced by analytical solutions obtained using the quasi-steady-state approximation for the concentration profiles within the droplet. In particular, the peroxide concentration inside the drop is approximated as

$$C_{\text{H}_2\text{O}_2}^{\text{in}}(r,t) \approx C_{\text{H}_2\text{O}_2}^{\text{out}}(t) \frac{a \sinh(3\alpha\, r/a)}{r \sinh(3\alpha)} \tag{S38}$$

where $\alpha = a/a^*$ is a dimensionless parameter characterizing the size of the drop relative to the reaction-diffusion length, $a^* = 3(D_{\text{H}_2\text{O}_2}/k_{\text{obs}}^{\text{in}})^{1/2} = 6.8$ μm. With this approximation, equation

---

[1]Note that the fraction plotted in Fig. 3c is actually $f/(1-\phi)$: the ratio between the catalase concentration in the dilute phase and the total catalase concentration. By contrast, the fraction f denotes the ratio between the amount (i.e., mass or number) of catalase present in the dilute phase and the total amount of catalase present in the system. Given the small estimated volume fraction of the condensed phase ($\phi \approx 0.001$), these ratios are nearly identical ($f/(1-\phi) \approx f$).

(S31) for the peroxide concentration in solution can be written as

$$\frac{dC_{\mathrm{H_2O_2}}^{\mathrm{out}}}{dt} = -\frac{k_{\mathrm{obs}}}{1-\phi}\left[f + (1-f)\left(\frac{1}{\alpha\tanh(3\alpha)} - \frac{1}{3\alpha^2}\right)\right]C_{\mathrm{H_2O_2}}^{\mathrm{out}} \tag{S39}$$

The effective rate constant for peroxide consumption (and therefore pH increase) depends on coacervate droplet size—that is, on the parameter α—as described by the bracketed term:

$$k_{\mathrm{obs}}\left[f + (1-f)\left(\frac{1}{\alpha\tanh(3\alpha)} - \frac{1}{3\alpha^2}\right)\right] = \begin{cases} k_{\mathrm{obs}} + O(\alpha^2) & \text{for } \alpha \ll 1 \\ fk_{\mathrm{obs}} + O(\alpha^{-1}) & \text{for } \alpha \gg 1 \end{cases} \tag{S40}$$

For small droplets ($\alpha \ll 1$), peroxide decomposition is reaction limited, and the apparent rate for the two-phase system is identical to that of free catalase. For large droplets ($\alpha \gg 1$), the reaction becomes diffusion-limited, and the apparent rate decreases with droplet size approaching a constant value as $\alpha \to \infty$. For such large droplets, the majority of peroxide decomposition takes place in the dilute phase catalyzed by the enzyme remaining therein; most of the catalase present in the condense phase is kinetically inaccessible to the peroxide fuel.

Figure S3b shows the transient profiles in the $\mathrm{H_2O_2}$ concentration and the pH as a function of radial position for droplets smaller and larger than the reaction diffusion length, $a^* = 3(D_{\mathrm{H_2O_2}}/k_{\mathrm{obs}}^{\mathrm{in}})^{1/2}$. For smaller drops ($a \ll a^*$), diffusion is fast, and concentration profiles are spatially uniform. For larger drops ($a \gg a^*$), reaction-induced pH changes are fast, and significant pH differences can arise between the drop interior and its surroundings. In this closed system, these pH differences are transient; the system evolves in time to a uniform pH determined by the acid-base equilibrium in the absence of peroxide.

2.2 Steady-State pH gradients

To maintain steady pH gradients between the inside and outside of the drop, it is necessary to supply $\mathrm{H_2O_2}$ and acid so as to maintain the peroxide concentration and pH in solution. In experiment, this type of "chemostatting" can be achieved using external feedback control whereby $\mathrm{H_2O_2}$ and acid (e.g., HCl) are added as needed to maintain the desired set points in the peroxide concentration and pH. Here, we consider an idealized scenario in which the concentrations at the drop surface ($r = a$) are held constant and equal to that of the well-stirred, chemostatted solution

$$C_{\mathrm{H^+}}(a,t) = H_0, \quad C_{\mathrm{OH^-}}(a,t) = \frac{K_{\mathrm{w}}}{H_0}, \quad C_{\mathrm{H_2O_2}}(a,t) = \frac{H_0 C_{\mathrm{p}}}{H_0 + K_{\mathrm{p}}}, \quad C_{\mathrm{HO_2^-}}(a,t) = \frac{K_{\mathrm{p}} C_{\mathrm{p}}}{H_0 + K_{\mathrm{p}}} \tag{S41}$$

These boundary conditions replace those of equation (S32).

Figure S4a shows the steady-state peroxide concentration and pH within small ($a = 1~\mu$m) and large ($a = 100~\mu$m) drops computed numerically. For drops larger than the reaction-diffusion length $a^* = 3(D_{\mathrm{H_2O_2}}/k_{\mathrm{obs}}^{\mathrm{in}})^{1/2} \approx 6.8~\mu$m, peroxide diffuses into the drop only a small distance of order a^* before being consumed by the enzymatic reaction. The local production of $\mathrm{OH^-}$ within this boundary layer causes the pH to increase throughout the drop interior. Note, however, that the magnitude of the pH increase is less than that observed in the transient system ($\Delta\mathrm{pH} = 0.87$ at steady-state vs. 1.4 in the transient system; cf. Figs. S3 and S4) owing to the diffusion of reaction
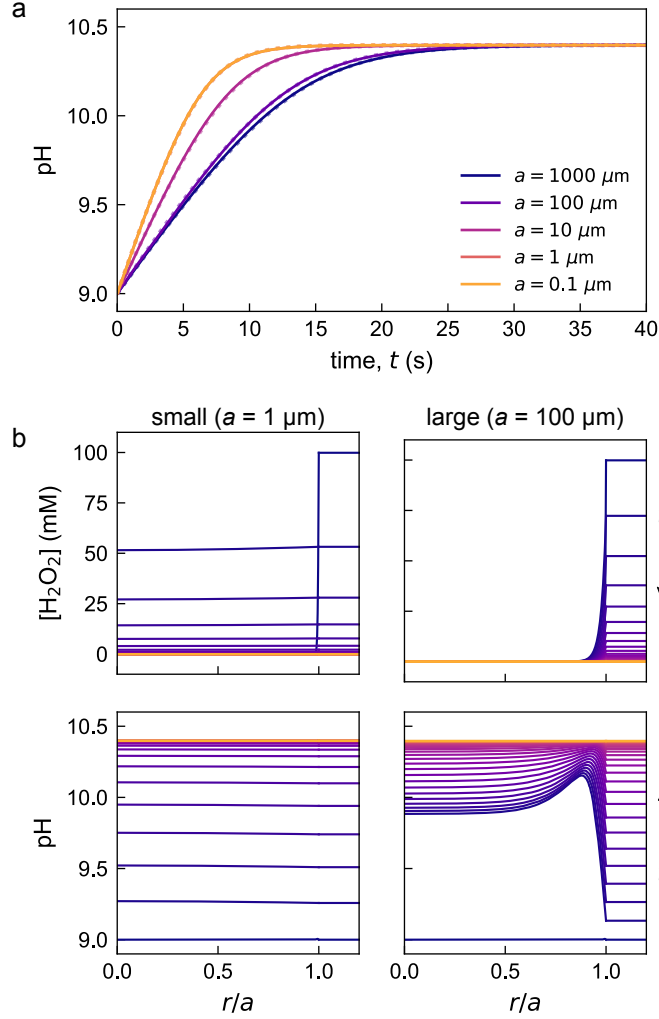
10

Figure S3: (a) Transient pH increase outside enzymatic drops of different sizes (cf. Fig. 5a). For drops smaller than the reaction-diffusion length $a^* = 3(D_{H_2O_2}/k_{obs}^{in})^{1/2} = 6.8\ \mu m$, there are no diffusion limitations, and the pH rise is controlled by the average rate k_{obs}. For larger drops, diffusion limits delivery and consumption of H_2O_2 inside the drop, and the pH rise is controlled by the outside rate k_{obs}^{out}. The solid curves denote the "exact" numerical results; the dashed curves denote analytical approximations based on equation (S16) using the effective rate constant (S40). (b) Transient profiles of peroxide concentration (top) and pH (bottom) as a function of radial position for enzymatic drops of radii smaller (left) and larger (right) than the reaction-diffusion length. The curves show regular time intervals of 1.2 s. The initial peroxide concentration is $C_p = 100$ mM and the initial pH is 9. Species diffusivities are $D_{H_2O_2} = D_{HO_2^-} = 1.43 \times 10^{-9}$ m^2/s, $D_{H^+} = 9.31 \times 10^{-9}$ m^2/s, and $D_{OH^-} = 5.27 \times 10^{-9}$ m^2/s. In the absence of reported values for $D_{HO_2^-}$, we approximate the diffusivity of HO_2^- by that of H_2O_2. The equilibrium and rate constants for the reactions are $K_w = 10^{-14}$ M^2, $K_p = 2.399 \times 10^{-12}$ M, $k_w^- = k_p^- = 1.4 \times 10^{11}$ M^{-1}s^{-1}, $k_{obs}^{in} = 270$ s^{-1}, and $k_{obs}^{out} = 0.240$ s^{-1}.

products out of the boundary layer and into solution. Nevertheless, significant pH differences can be maintained at steady-state for sufficiently large drops (Fig. S4b).
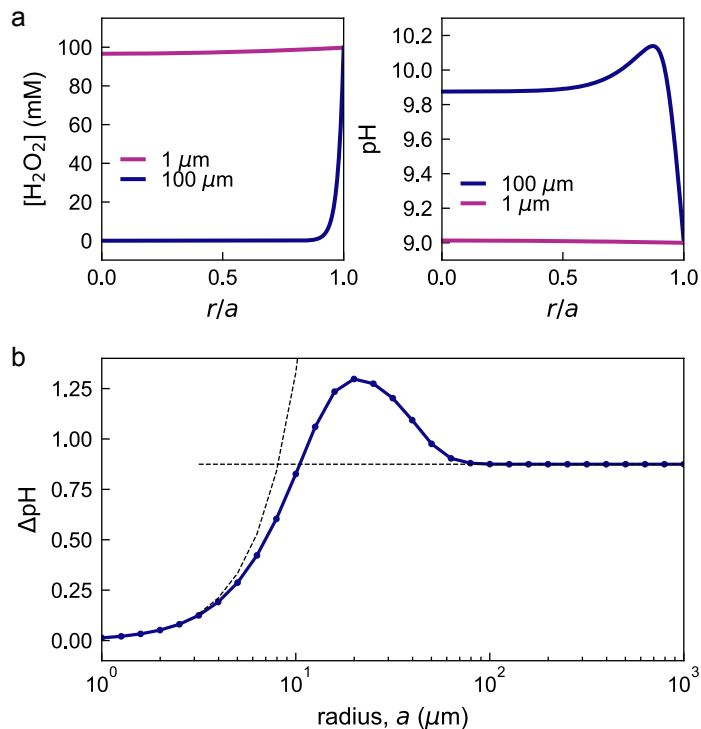

Figure S4: (a) Steady-state profiles of peroxide concentration (left) and pH (right) as a function of radial position for enzymatic drops of radii smaller ($a = 1 \ \mu m$) and larger ($a = 100 \ \mu m$) than the reaction-diffusion length $a^* = 6.8 \ \mu m$. (b) Steady pH difference between the drop interior ($r = 0$) and the surrounding solution as a function of drop radius. The asymptotic behavior is approximated as $\Delta pH \approx 0.87$ for large drops and $\Delta pH \approx a^2/75.3 \ \mu m^2$ for small drops. Model parameters are the same as those used in Fig. S3.

3   Generic model of activity-induced destabilization

The activity-induced destabilization of catalytic coacervate droplets is not limited to catalase and hydrogen peroxide. Here, we consider a generic reaction of the form $A \to B$, in which a chemical "fuel" A reacts to form a destabilizing product B. When the concentration of B exceeds a critical amount C_B^*, the coacervate drop becomes unstable and undergoes dissolution. Using reaction-diffusion models analogous to those described in Section 2, we identify the necessary conditions to achieve this instability.

3.1   Drop stability at steady-state

We first consider the steady-state concentration profiles in a spherical drop of radius a immersed in a well-stirred solution. The concentrations of A and B in solution are maintained constant—for example, using a chemostat. The concentrations inside the drop C_A and C_B obey the following reaction-diffusion equations

$$
\begin{aligned}
\frac{\partial C_A}{\partial t} &= \frac{D_A}{r^2}\frac{\partial}{\partial r}\left(r^2\frac{\partial C_A}{\partial r}\right) - k_{\text{in}}C_A \\
\frac{\partial C_B}{\partial t} &= \frac{D_B}{r^2}\frac{\partial}{\partial r}\left(r^2\frac{\partial C_B}{\partial r}\right) + k_{\text{in}}C_A
\end{aligned}
\tag{S42}
$$

where D_A and D_B are the respective diffusivities of the two species inside the drop, and k_{in} is the reaction rate constant inside the drop. The boundary conditions are

$$
0 = \left.\frac{\partial C_i}{\partial r}\right|_{r=0} \quad \text{and} \quad C_i(r=a) = C_i^{\text{out}} \quad \text{for } i = \{A, B\}
\tag{S43}
$$

At steady-state, the concentration profiles in the drop are

$$
C_A(r) = C_A^{\text{out}}\frac{a\sinh(3\alpha r/a)}{r\sinh(3\alpha)}
\tag{S44}
$$

$$
C_B(r) = C_B^{\text{out}} + C_A^{\text{out}}\frac{D_A}{D_B}\left(1 - \frac{a\sinh(3\alpha r/a)}{r\sinh(3\alpha)}\right)
\tag{S45}
$$

where $\alpha = \frac{1}{3}\sqrt{k_{\text{in}}a^2/D_A}$ is a dimensionless parameter that characterizes the size of the drop relative to the reaction-diffusion length.[2]   The drop is stable when the concentration of the destablizing product $C_B(r)$ everywhere is below the threshold value C_B^*. As $C_B(r)$ is maximal at $r = 0$, this condition for instability is

$$
C_B^* < C_B(0) = C_B^{\text{out}} + C_A^{\text{out}}\frac{D_A}{D_B}\left(1 - \frac{3\alpha}{\sinh(3\alpha)}\right)
\tag{S46}
$$

To destabilize large droplets but not small droplets, we require the following conditions

$$
C_B^{\text{out}} < C_B^* < C_B^{\text{out}} + C_A^{\text{out}}\frac{D_A}{D_B}
\tag{S47}
$$

---

[2]The factor of 3 is introduced such that the crossover from small to large drops is centered on $\alpha = 1$ (see below).

which ensures that $C_B^* = C_B(0)$ for some finite droplet radius a. In particular, the maximum stable droplet size $a_{\max}$ can be approximated as

$$a_{\max} = \begin{cases} a^* \left(\frac{2D_B(C_B^* - C_B^{\text{out}})}{3D_A C_A^{\text{out}}} \right)^{1/2} & \text{for } \alpha \ll 1 \\ a^* & \text{for } \alpha \gg 1 \end{cases} \tag{S48}$$

where $a^* = 3(D_A/k_{\text{in}})^{1/2}$ is the reaction-diffusion length.

3.2 Transient destabilization of large drops

When the solution outside the drop is not chemostatted, the concentration of destabilizing product $C_B^{\text{out}}(t)$ grows in time. Depending on the asymptotic concentration $C_B^{\text{out}}(t \to \infty)$, drops are stable ($C_B^{\text{out}} < C_B^*$) or unstable ($C_B^{\text{out}} > C_B^*$) regardless of their size. Even when drops are stable at long times, it remains possible that large drops can undergo transient destabilization when the local concentration of B exceeds the threshold. Here, we consider this possibility using the pseudo-steady-state approximation and identify the necessary conditions for such transient destabilization.

For a collection of spherical drops with total surface area A dispersed in a solution of volume V, the concentrations in the well-mixed solution evolve as

$$\frac{dC_A^{\text{out}}}{dt} = -k_{\text{out}} C_A^{\text{out}} - \frac{AD_A}{V} \left. \frac{\partial C_A}{\partial r} \right|_{r=a} \tag{S49}$$

$$\frac{dC_B^{\text{out}}}{dt} = k_{\text{out}} C_A^{\text{out}} - \frac{AD_B}{V} \left. \frac{\partial C_B}{\partial r} \right|_{r=a} \tag{S50}$$

where k_{out} is the rate constant in solution, and $V/A = a/3$ for monodisperse drops of radius a. The solute concentrations change due to reaction in solution and diffusion to/from the drops. To facilitate our analysis, we assume that the concentrations in the drop approach their steady-state profiles quickly relative to the concentration changes in solution (see below). We can then approximate the solute fluxes at the drop surface by their steady-state values such that

$$\frac{dC_A^{\text{out}}}{dt} = -\frac{dC_A^{\text{out}}}{dt} = -kC_A^{\text{out}} \quad \text{with} \quad k = k_{\text{out}} + k_{\text{in}} \left(\frac{1}{\alpha \tanh(3\alpha)} - \frac{1}{3\alpha^2} \right) \tag{S51}$$

Starting from initial values $C_{A,0}^{\text{out}}$ and $C_{B,0}^{\text{out}}$, the concentrations evolve as

$$\begin{aligned} C_A^{\text{out}}(t) &= C_{A,0}^{\text{out}} e^{-kt} \\ C_B^{\text{out}}(t) &= C_{B,0}^{\text{out}} + C_{A,0}^{\text{out}}(1 - e^{-kt}) \end{aligned} \tag{S52}$$

Substituting this result into equation (S46), the concentration of destabilizing product at the drop centers evolves as

$$C_B(0,t) = C_{B,0}^{\text{out}} + C_{A,0}^{\text{out}} - C_{A,0}^{\text{out}} \left[1 - \frac{D_A}{D_B} \left(1 - \frac{3\alpha}{\sinh(3\alpha)} \right) \right] e^{-kt} \tag{S53}$$

At long times, the concentration approaches $C_{B,0}^{\text{out}} + C_{A,0}^{\text{out}}$ when all of the fuel is consumed. To achieve transient drop destabilization, the concentration of B at short times must rise above this asymptotic value which requires that

$$\frac{D_B}{D_A} < 1 - \frac{3\alpha}{\sinh(3\alpha)} \tag{S54}$$

14

Even for large drops ($\alpha \to \infty$), for which the right hand side approaches its maximal value of 1, this condition implies that the diffusivity of the destabilizing product must be less than that of the fuel to achieve transient destabilization. This condition is not satisfied in the catalase-peroxide system since the product—namely, OH^-—diffuses faster than the reactant H_2O_2. As a result, the transient pH in Figure S3 does not rise above its asymptotic value.

The validity of the pseudo-steady-state approximation (PSSA) requires that the time required to establish the concentration profiles inside the drops is fast compared to concentration changes outside the drops. The relaxation rate for concentrations of A and B inside the drop are $k_{in} + \pi^2 D_A/4a^2$ and $\pi^2 D_B/4a^2$, respectively. The PSSA is appropriate when these rates are faster than the rate k of equation (S51), which describes the changing concentrations in solution. For species A, which evolves independently of species B, this condition implies that $k_{in} \gg k_{out}$—the rate of the reaction inside the drop must be faster than that in solution. Here, this condition is achieved by enriching the drop with an enzyme that catalyzes the reaction. For species B, the PSSA breaks down for large drops ($\alpha \gg 1$) due to slow diffusive relaxation inside the drop. The transient depletion of B from the reaction zone near the drop surface into the droplet interior (neglected by the PSSA) makes transient destabilization less likely to occur.

3.3   Experimental results on transient destabilization

The model predicts that large drops are unlikely to undergo transient destabilisation in the catalase/ DEAE-dextran system. We tested this prediction by the addition of H_2O_2 fuel to a coacervate dispersion containing drops of different sizes at an initial pH of 8.5. The addition of 100 mM H_2O_2 caused the pH to increase to $\sim$9.5, which is below the threshold value required for coacervate dissolution. Consistent with expectations of the model, coacervate size distributions in water before and after the reaction reveal no significant differences (Fig. S5a); similar results are obtained in a buffered control (Fig. S5b).

Experimental Details.   Individual solutions of 0.25 mg/mL catalase and 0.25 mg/mL DEAE-dextran in water at pH 9 were prepared. 14.1 mL of 0.25 mg/mL catalase and 0.9 mL of 0.25 mg/mL DEAE-dextran were added to a glass vial and vortexed to obtain a coacervate solution at 0.94 mass fraction of catalase. After mixing, the pH was readjusted to 9 and the glass vial was sealed using parafilm. Two such vials were prepared and left on a horizontal stirrer at room temperature. After 2.5 h, microscopy images of the coacervates were taken by removing 20 μL from the vial into uncovered imaging chambers created using press-to-seal silicone isolators on glass slides (using a lens of magnification 20X). The pipetted solution was left undisturbed for 1 min to allow the condensed phase to settle at the bottom of the chamber. Microscopy images were taken in triplicate for each vial using three imaging chambers and two different locations in each chamber.

The area of the coacervates in the images was measured using ImageJ. The images were thresholded by conversion to a binary image wherein the condensed phase was separated from the background. Smoothing of the image was done using the Gaussian blur filter ($\sigma = 2$ pixels). The images were again converted into binary images, and the area of each continuous coacervate 'blob' was calculated using the *Analyze Particles function*. Each such blob is represented by a single point
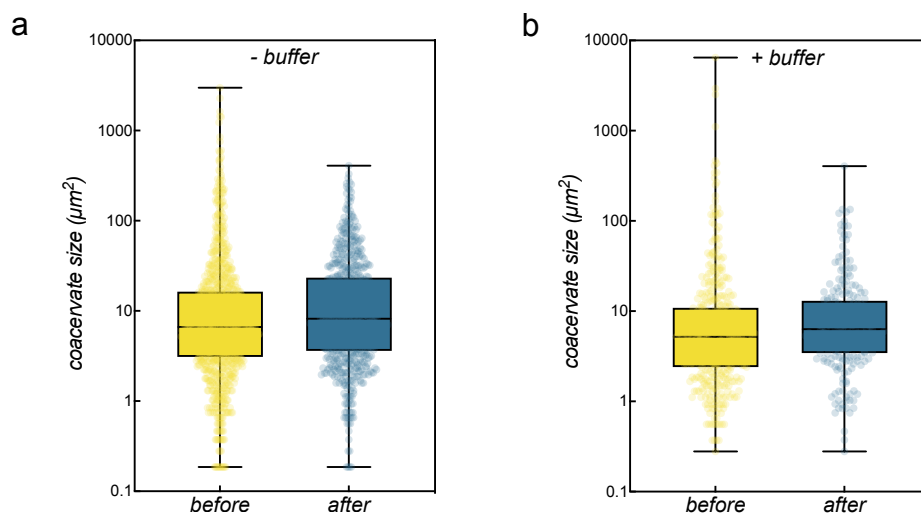
Figure S5: (a) Size distributions of coacervates at pH 9 before the addition of 100 mM H_2O_2 and after its enzymatic decomposition at pH 9.5 in water. (b) Control experiments show coacervate sizes in 50 mM Tris at before the reaction at pH 9 and after the reaction at pH 9.5. Coacervate sizes on an area basis are obtained from optical microscopy images of droplets sedimented onto a glass substrate. The area corresponding to a coacervate with a critical radius of 7 μm is 154 μm^2.

in the scattered boxplot (Fig. S5a, before).

To the coacervate dispersion, H_2O_2 was added to initiate the reaction-induced pH increase. To maintain coacervate stability, the initial pH of the coacervate solution was adjusted to 8.5 using 0.1 M HCl prior the reaction. A 10 M H_2O_2 solution in water was adjusted to pH 8.5 using 10 M NaOH and added to the coacervate solution to achieve a final concentration of 0.1 M H_2O_2. During the reaction, the pH rose by approximately 1 unit to $\sim$9.5. Once the reaction was complete, microscopy images were taken in the same manner as above (Fig. S5a, after).

As a control experiment, the above procedure was repeated in the presence of buffer. Catalase / DEAE-dextran coacervates were prepared in 50 mM Tris pH 9 in the same manner as above. After taking the microscopy images, the pH of the coacervate solution in the vial was adjusted to 8.5 using 6 M HCl. H_2O_2 was added such that its final concentration in the vial was 0.1 M. Due to the presence of the buffer, the reaction did not cause an increase in pH. Instead, the pH of the solution was increased manually to 9.5 by addition of 10 M NaOH. Microscopy images were taken in the same manner as described above (Fig. S5b).

4 Experimental data on catalase activity

4.1 Absorbance assay for catalase activity

We measured the specific activity of catalase using the standard spectrophotometic assay to confirm that it falls within the range specified by the supplier. Catalase from bovine liver purchased from Sigma Aldrich (C9322) is reported to have a specific activity of 2000-5000 units/mg of protein. We measured the absorbance of H_2O_2 at 240 nm as a function of time for a solution containing 1.7 μg/mL catalase and 10.5 mM H_2O_2 in phosphate buffer at pH 7 (Fig. S6a). The specific activity was calculated based on the initial reaction velocity defined as

$$v_o = \frac{\Delta A_{240}}{\varepsilon \ell \Delta t} \tag{S55}$$

where $\varepsilon = 42.4$ $M^{-1}cm^{-1}$ is the extinction coefficient of H_2O_2 at 240 nm, and $\ell = 1$ cm is the optical path length. From the measured velocity of $v_o = 3.8$ mM/min, the specific activity is 2290 units/mg protein, which is within the expected range.

Previous studies of catalase kinetics[2] report a second order rate constant of $k_s = 2.0 \times 10^7$ $M^{-1}s^{-1}$ at pH 7 for H_2O_2 concentrations up to 30 mM. We fit the transient absorbance data in Figure S6a with an exponential decay to determine the apparent first order rate constant of $k_{obs} = 0.68$ min^{-1} for an enzyme concentration of 1.7 μg/mL. This value corresponds to a second order rate constant $k_s = 1.6 \times 10^6$ $M^{-1}s^{-1}$, which is ca. 10 times lower than the value reported by Beers & Sizer.[2] We attribute this discrepancy to differences in the enzyme purity.

We used the same absorption-based assay to determine the first order rate constant for peroxide
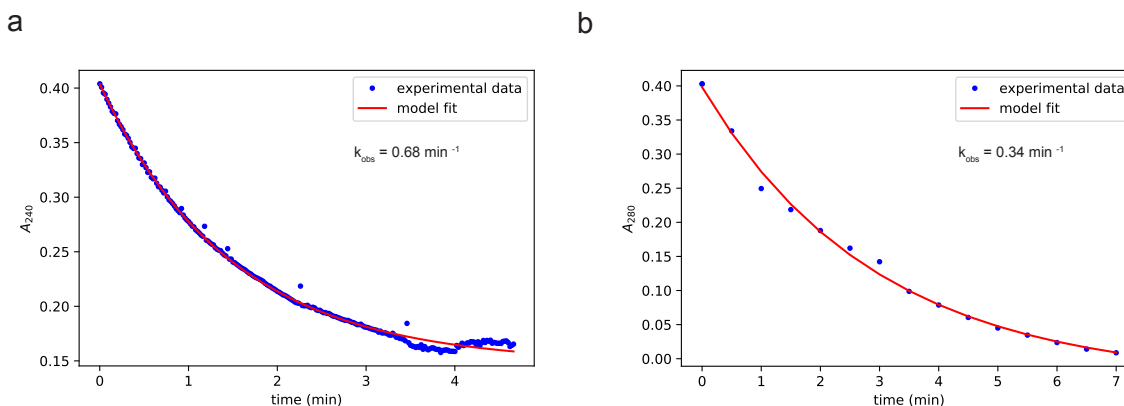

Figure S6: Absorbance assay for catalase activity. (a) Standard assay of catalase activity at pH 7 in 50 mM phosphate buffer. Markers denote the measured absorbance at 240 nm as a function of time for a catalase concentration of 1.7 μg/mL and an H_2O_2 concentration of 10.5 mM. The curve shows the least-squares fit to the data using a exponential decay model with rate $k_{obs} = 0.68$ min^{-1}. The initial reaction velocity is $v_o = 3.8$ mM H_2O_2 per minute, which corresponds to an enzyme activity of 2290 units/mg protein. (b) Catalase activity assay at pH 9. Here, the catalase concentration is 4.1 μg/mL and the H_2O_2 concentration is 100 mM. The assay is carried out in 1 mM Tris pH 9. The curve shows the best exponential fit with rate $k_{obs} = 0.34$ min^{-1}.

decomposition under conditions corresponding to the experiments reported in the main text—namely, 100 mM H_2O_2 and pH 9 (Fig. S6b). Absorbance readings at 280 nm (extinction coefficient of H_2O_2 at 280 nm is 4.2 $M^{-1}cm^{-1}$) were taken every 30 seconds to allow for vortex mixing to remove oxygen bubbles from the walls of the cuvette. The observed rate constant is estimated to be $k_{obs} = 0.34$ min^{-1} for 4.1 μg/mL catalase, which corresponds to a second order rate constant $k_s = 3.3 \times 10^5$ $M^{-1}s^{-1}$. The lower rate constant at higher pH and peroxide concentration is attributed to reduced activity[7] of the enzyme at high pH and/or substrate inhibition[8] by H_2O_2.

4.2   pH assay for catalase activity

Catalase activity can be also be quantified from transient pH data following the addition of catalase to H_2O_2 solutions (Fig. S7). We measured the time scale t^* using linear regression of the transient pH data within finite time windows satisfying the condition $pH_0 < pH(t) < pH_0 + \frac{1}{3}\Delta pH$, corresponding to the initial reaction rate. From the measured time scale and pH increase, the apparent rate constant k_{obs} was calculated using equation (S27). Dividing by the specified enzyme concentration, we obtained the second order rate constant k_s summarized in Table SI. For the data in Fig. S7, the observed time scale $t^* = 6.68$ min and pH increase $\Delta pH = 1.41$ imply a second order rate constant $k_s = 2.5 \times 10^5$ M^{-1} s^{-1}, which agree with obtained from the absorbance assay under similar conditions.

By contrast, the results of the pH assay for higher catalase concentrations used in coacervate experiments indicate a somewhat higher catalytic rate (Table SI). One possible explanation for this difference is increased inhibition of the enzyme by comparatively long periods of exposure to high H_2O_2 concentrations when the assay is conducted at a lower enzyme concentration. According to Lardinois et al.,[8] bovine liver catalase shows reduced reaction rates upon exposure to H_2O_2 concen-
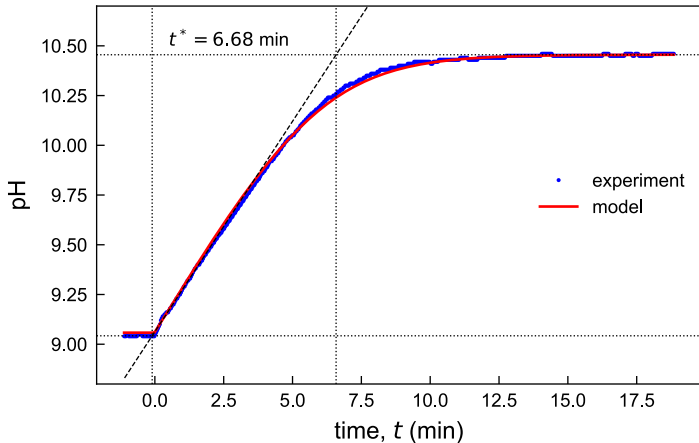

Figure S7: pH assay for catalase activity. The markers show the measured pH as a function of time for a 8.1 μg/mL catalase solution upon addition of 100 mM H_2O_2. The solid curve shows the theoretical prediction of equation (S26) with a fitted rate constant $k_{obs} = 0.550$ min^{-1}. The characteristic time scale based on the geometric construction described in Fig. 2c of the main text is $t^* = 6.68$ min. This observed time scale agree closely to the 6.14 min predicted by equation (S27) based on the observed pH increase $\Delta pH = 1.41$ and the fitted k_{obs}.

18

trations greater than 75 mM for more than half a minute. The time scale for H_2O_2 decomposition is ca. minutes when the catalase concentration is 8.1 μg/mL as opposed to a seconds for 220 μg/mL catalase.

Absorbance Assay 4.1 μg/mL cat. k_s (M^{-1} s^{-1})	pH Assay 8.1 μg/mL cat. k_s (M^{-1} s^{-1})	pH assay 220 μg/mL cat. k_s (M^{-1} s^{-1})
1.87×10^5	2.51×10^5	6.77×10^5
2.45×10^5	1.39×10^5	4.46×10^5
3.31×10^5	1.82×10^5	5.67×10^5
$-$	$-$	4.88×10^5
$(2.54 \pm 0.59) \times 10^5$	$(1.91 \pm 0.46) \times 10^5$	$(5.45 \pm 0.88) \times 10^5$

Table SI: Comparison of second order rate constants k_s for enzymatic decomposition of H_2O_2 by catalase obtained using the absorbance assay (Section 4.1) and the pH assay (Section 4.2). The absorbance assay (left column) was conducted using 100 mM H_2O_2 at pH 9 with catalase concentration 4.1 μg/mL. The pH assay was conducted using 100 mM H_2O_2 at initial pH 9 with catalase concentrations of 8.1 μg/mL (middle column) and 220 μg/mL (right column). The last row shows the arithmetic average and standard deviation for the values in each column.

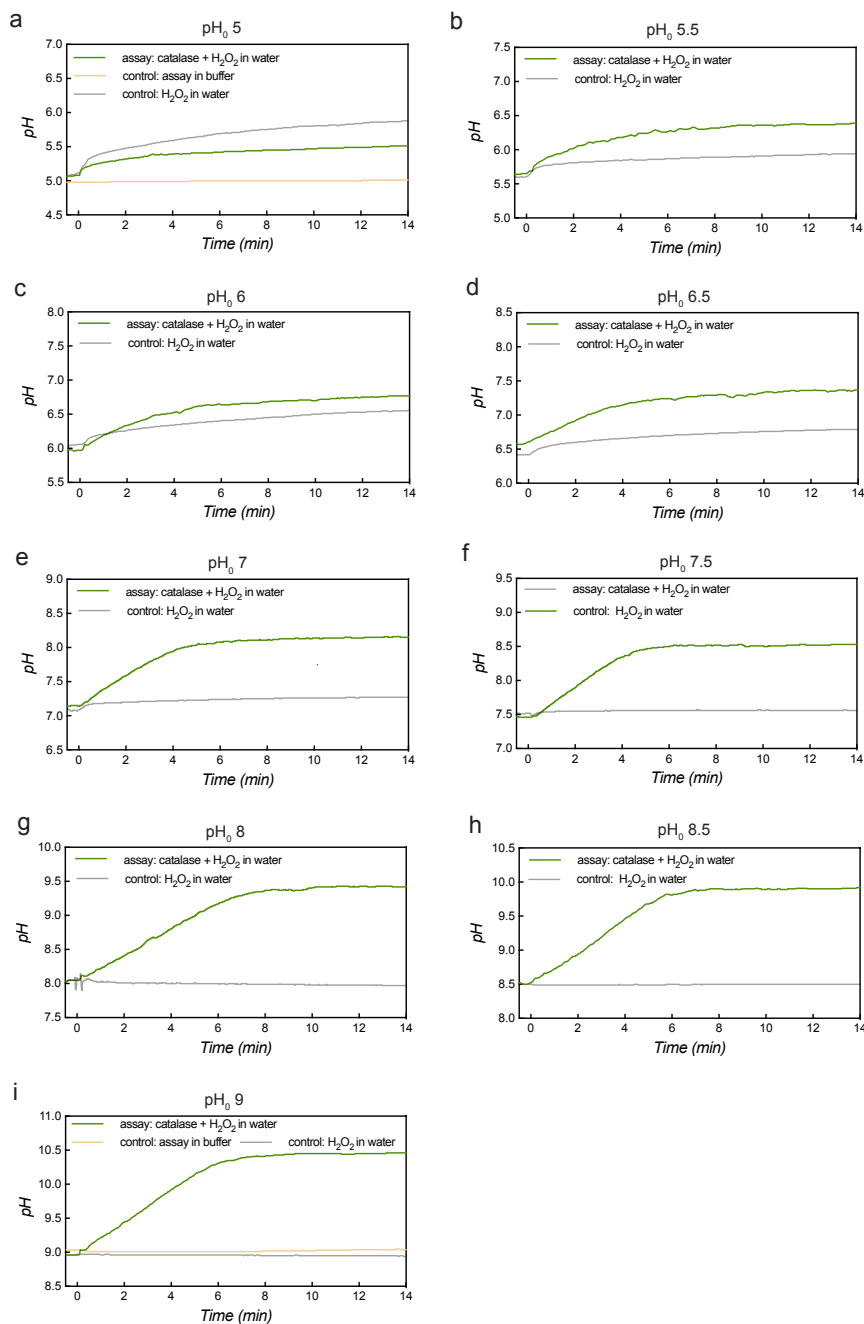## 4.3 Transient pH data on the effect of initial pH (Fig. 2a)

Figure S8: Transient pH increase upon addition of catalase to 100 mM H_2O_2 solutions at different initial pH values: (a) 5, (b) 5.5, (c) 6, (d) 6.5, (e) 7, (f) 7.5, (g) 8, (h) 8.5, (i) 9. In each assay, the enzyme is added at 0 s; the total enzyme concentration is 8.1 μg/mL. Each plot shows the result of a single assay (green curve) at a given initial pH as well as a control (grey curve) without added catalase. Plots (a) and (i) corresponding to initial pH values of 5 and 9 show an additional control (yellow curve) where the reaction-induced pH increase is inhibited by 50 mM phosphate and 100 mM Tris buffers, respectively. The nine assays and controls shown here were repeated twice more to obtain the data presented in Figure 2a.

4.4 Transient pH data on the effect of initial H_2O_2 concentration (Fig. 2b)
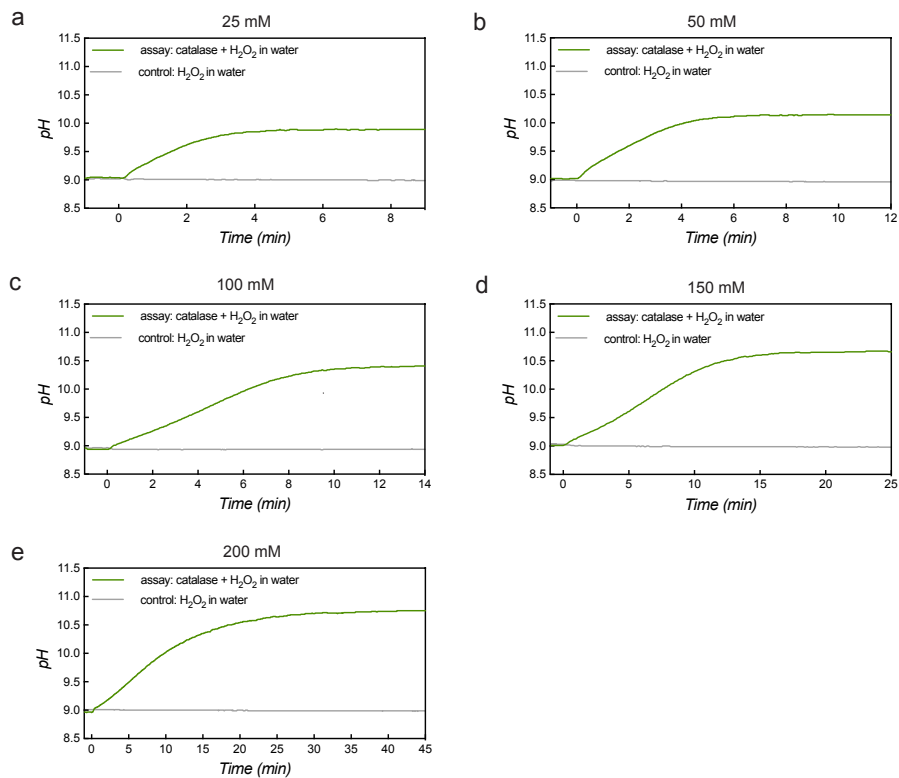

Figure S9: Transient pH increase upon addition of catalase to H_2O_2 solutions of different concentrations: (a) 25 mM, (b) 50 mM, (c) 100 mM, (d) 150 mM, (e) 200 mM. In each assay, the enzyme is added at 0 s; the total enzyme concentration is 8.1 μg/mL; the initial pH is 9. Each plot shows the result of a single assay (green curve) at a given H_2O_2 concentration as well as a control (grey curve) without added catalase. The five assays and controls shown here were repeated twice more to obtain the data presented in Figure 2b.

5 Phase separation of catalase

5.1 Estimating the charge fraction

The amino acid sequence used for the calculation of protein charge corresponded to Gene ID: 531682 obtained from the NIH database (`https://www.ncbi.nlm.nih.gov/gene/531682#bibliography`). The molar mass of the catalase tetramer is estimated to be 240,000 Da as calculated using the above amino acid sequence. The charge on catalase was estimated by applying the Henderson Hasselbach equation to the pKa values of the isolated amino acid residues.[9] Similarly, the charge of DEAE-dextran was estimated by applying the Henderson Hasselbach equation to the isolated amines present on DEAE-dextran.[10]

5.2 Quantifying the size of coacervate droplets

Coacervates formed by catalase and DEAE-dextran at a mixing ratio corresponding to 0.94 mass fraction of catalase in 10 mM Tris pH 9 and a total macromolecular concentration of 0.25 mg/mL are less than 1 μm in diameter. We analyzed the microscopy images of the coacervate drops imaged at 15 min and 1 h post mixing in ImageJ to estimate the diameter from the measured area of the coacervate drops. At each time point, we analyzed two images and the average droplet area of 10 drops in each image is estimated to be ~ 0.3 μm^2. The diameter of the coacervate drops is thus less than 1 μm.
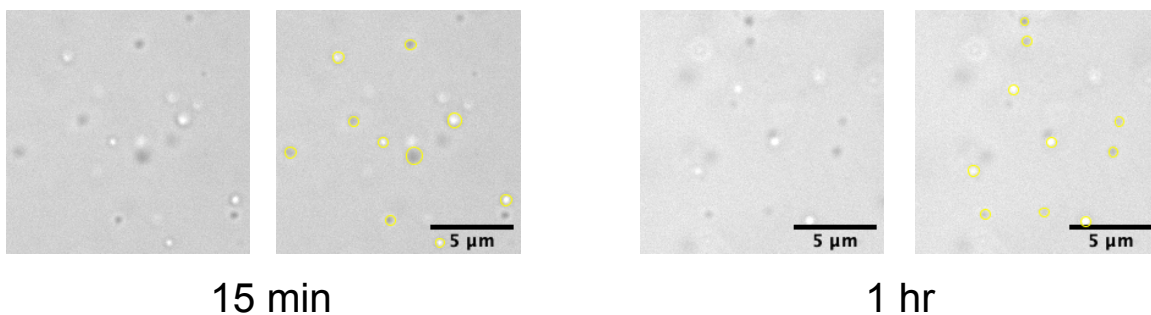

15 min   **1 hr**

Figure S10: Microscopy images of coacervate drops imaged at 15 min and 1 h after mixing catalase and DEAE-dextran in 10 mM Tris buffer at pH 9. The total macromolecular concentration is 0.25 mg/mL; the mass fraction of catalase is 0.94. The left image and right image in each column represents the microscopy image before and after analysis respectively.

6 Catalytic activity of catalase/DEAE-dextran coacervates

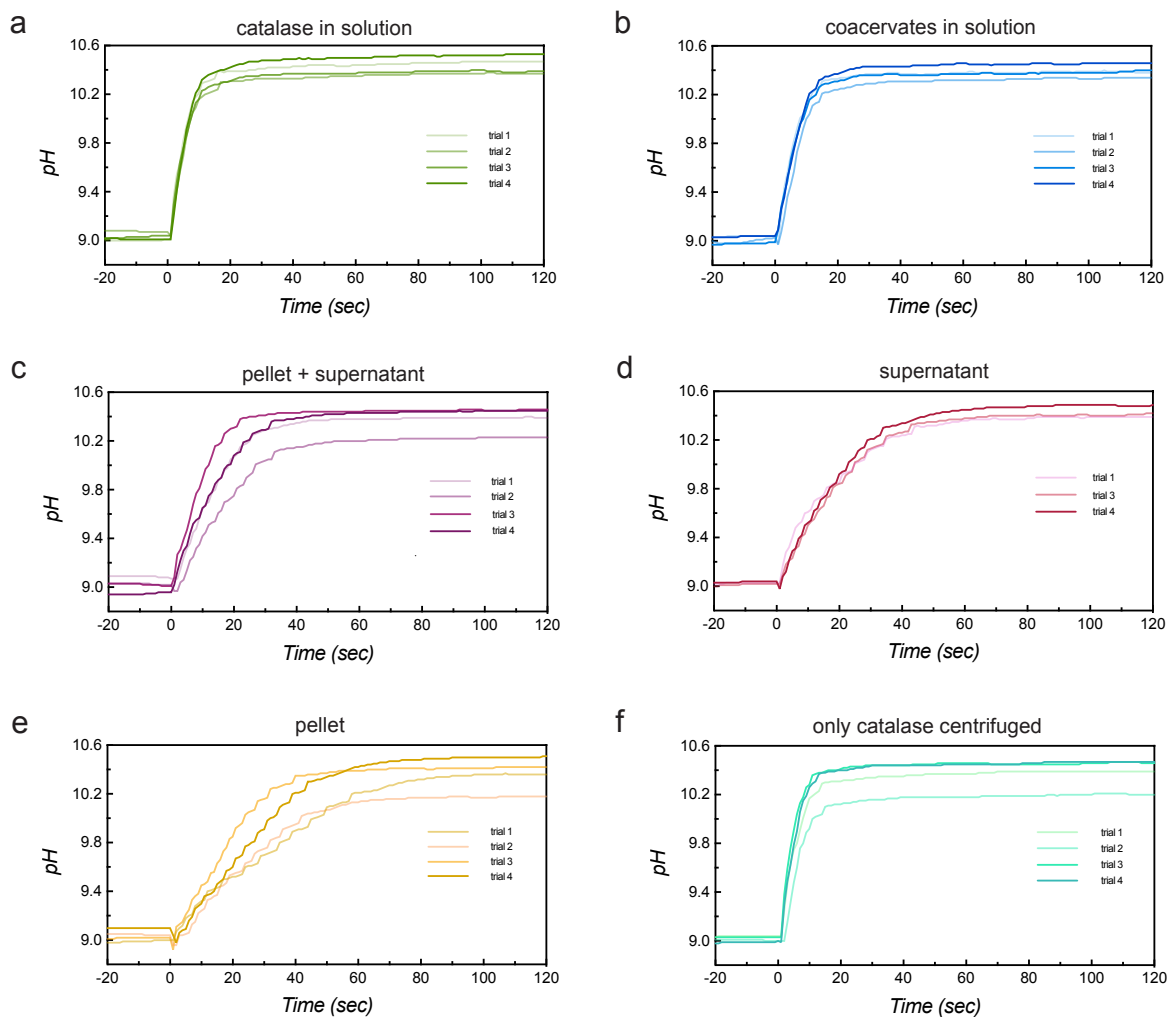## 6.1 Transient pH data for active coacervates (Fig. 5a)

Figure S11: Transient pH data corresponding to the experiments described in Figure 5 of the main text: (a) 'catalase in solution', (b) 'coacervates in solution', (c) 'pellet + supernatant', (d) 'supernatant', (e) 'pellet', (f) 'only catalase centrifuged'. The last control experiment (f) is identical to that in (a) except that the solution is centrifuged at 4000 rpm for 30 min. As expected, there is no significant difference between the measured pH increase for experiments (a) and (f). In each assay, H_2O_2 was added at 0 sec to solutions at initial pH 9 to obtain an initial H_2O_2 concentration of 100 mM in each assay.

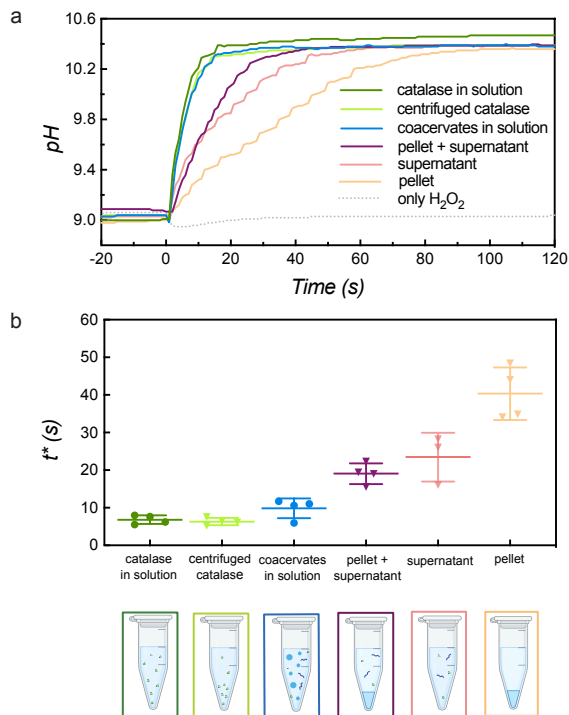## 6.2 Transient pH increase in coacervates of two different sizes (Fig. 5).

Figure S12: (a) Representative pH measurements as a function of time for H_2O_2 decomposition by free enzyme in solution ('catalase in solution'), a centrifuged catalase solution as a control to demonstrate that catalase forms pellets upon centrifugation only in the presence of DEAE-dextran ('centrifuged catalase'), micron scale coacervate droplets ('coacervates in solution'), a macro-scale coacervate pellet obtained by centrifugation (pellet + supernatant) and for the isolated individual dilute ('supernatant') and dense phase ('pellet') of the centrifuged dispersion. The initial pH is 9; the initial peroxide concentration is 100 mM; the catalase concentration is 0.224 mg/mL; the mass fraction of catalase is 0.94 for the mixed samples. A control (only H_2O_2) shows no pH increase in the absence of catalase. (b) Comparison of t^* values obtained from pH versus time data of the type shown in (a). Error bars represent ± 1 standard deviation above/below the mean of replicates.

6.3 Measured t^* values for pH increase in coacervates (Fig. 5b)

catalase in solution $t^*(s)$	coacervates in solution $t^*(s)$	pellet + supernatant $t^*(s)$	supernatant $t^*(s)$	pellet $t^*(s)$	only catalase centrifuged $t^*(s)$
5.55	5.99	19.42	16.09	48.41	6.51
7.67	10.66	22.30	—	34.11	7.56
6.25	11.08	15.58	28.3	34.86	5.18
7.98	11.77	19.03	26.07	44.02	6.11
6.9 ± 1.0	9.9 ± 2.3	19.1 ± 2.4	23.5 ± 5.3	40.4 ± 6.1	6.3 ± 0.9

Table SII: Characteristic time scales t^* for the transient pH increase in each of the experiments presented in Figure S12 and plotted in Figure 5b. The last row shows the arithmetic average and standard deviation for the values in each column.

6.4 Consistency checks on t^* Values

Check 1. From the reaction-diffusion model in Section 2, the effective reaction rate for peroxide decomposition in the 'pellet + supernatant' is predicted to be indistinguishable from that of the 'supernatant' alone

$$k_{\text{obs}}^{\text{pellet+supernatant}} \approx k_{\text{obs}}^{\text{supernatant}} \tag{S56}$$

This approximate equality follows from equation (S40) with $\alpha \gg 1$ for macroscopic droplets much larger than the reaction-diffusion length. Consistent with this prediction, the time scales t^* for these two experiments are statistically indistinguishable as evidenced by a p-value of 0.36 for a two-sided t-test with unequal variance. Pooling these data, we obtain a mean t^* value of 21 ± 4.5 s and an associated rate constant $k_{\text{obs}}^{\text{out}} = 0.16 \pm 0.034$ s^{-1} using equation (S27).

Check 2. In the supernatant, the effective reaction rate for peroxide decomposition is predicted to be

$$k_{\text{obs}}^{\text{supernatant}} = k_{\text{obs}}^{\text{out}} = \frac{f}{1-\phi} k_{\text{obs}} \tag{S57}$$

where $f \approx 0.47$ is the fraction of catalase present in the dilute phase, and $\phi \approx 0.001$ is the estimated volume fraction of the condensed phase. Pooling the data from columns 1 and 6 in Table SII, the mean rate constant for catalase in solution is $k_{\text{obs}} = 0.51 \pm 0.074$ s^{-1}. The mean rate constant for the supernatant is estimated above to be $k_{\text{obs}}^{\text{out}} = 0.16 \pm 0.034$ s^{-1} based on columns 3 and 4 of Table SII. The ratio between the two rate constants is estimated to be 0.31 ± 0.082, which is less than the expected value of 0.47. We hypothesize that this discrepancy is due to a combination of factors including the incomplete separation of the labelled enzyme from the unreacted fluorophore, differences in ionic strength, and experimental uncertainty.

Incomplete separation of the fluorescently labeled enzyme from the unreacted fluorophore would lead to an overestimate of the enzyme concentration in the supernatant and thereby the fraction f. The reported value of f as 0.47 is the maximum value of the fraction of catalase present in the

dilute phase at 0.94 mass fraction of enzyme assuming a 100% separation efficiency of the NAP-25 column. The fraction of catalase present in the dilute phase at this mass fraction would be lower at lower separation efficiencies. At a 95% separation efficiency, we estimate that the value of f would decrease from 0.47 to 0.29.

Purification of the labeled enzyme was performed using NAP-25 Cytiva columns packed with Sephadex G-25 resin. Purified samples of fluorescently labeled catalase of 0.5 mg/mL concentration were used for partitioning assays (see Methods). We calculated the concentration of dye in the purified labeled solution by comparing the absorbance of the labeled enzyme solution at 494 nm to the calibration curve for pure Alexa Fluor dye at 494 nm (the absorbance of the unlabelled enzyme at 494 nm is negligible). The dye concentration at a particular mixing ratio was calculated by multiplying the concentration of dye in the purified labeled solution calculated as mentioned above with the mass fraction of catalase at that mixing ratio.

The reported fraction of catalase present in the dilute phase as a function of mixing ratio (Fig. 3c) was calculated by dividing the concentration of dye remaining in the supernatant after centrifugation of the coacervate solution at a particular mixing ratio by the dye concentration present at that mixing ratio in the absence of DEAE-dextran. This calculation assumes that all the dye present in the supernatant is associated with catalase (corresponding to 100% separation efficiency via the NAP-25 column). On the basis of this assumption, the reported fraction of catalase present in the dilute phase at 0.94 mass fraction of enzyme (f) is 0.47.

We estimate the fraction of catalase present in the dilute phase at a lower separation efficiency by calculating the molar ratio of dye to enzyme present before and after separation. Before separation, the initial molar ratio of the total dye added to the enzyme was 20:1 (see methods). After separation using a single NAP-25 column, the molar ratio of the total dye to enzyme present in the purified labeled catalase samples (0.5 mg/mL) was 3.6. Here, the total dye concentration includes the dye conjugated to the enzyme as well as the unreacted free dye. Assuming a 95% efficiency of separation of the unreacted fluorophore from the fluorescently labeled enzyme, the molar ratio of dye associated with the enzyme to the total enzyme present in the 0.5 mg/mL purified labeled catalase solution is estimated to be 2.7. This means that for every mole of labeled enzyme present in the purified enzyme solution, there are 2.7 molar equivalents of fluorophore present that are attached to the enzyme along with 0.9 equivalents of unreacted fluorophore.

Taking into account the potential 0.9 equivalents of unreacted Alexa Fluor dye that would be left in the supernatant for every mole of catalase present at 0.94 mass fraction of enzyme (0.5 mg/mL total macromolecular concentration), the actual fraction of catalase present in the dilute phase at this mass fraction is estimated to be 0.29.

Differences in the ionic strength between catalase partitioning experiments (Fig. 3c) and coacervate activity measurements (Fig. 5) may also contribute to deviations from the expectations of equation (S57). Catalase partitioning experiments using fluorescently labeled enzyme were performed in 10 mM Tris buffer, while coacervate activity measurements of t^* were conducted in water to prevent buffering of the pH increase. Increasing the ionic strength leads to the destabilization of coacervates due to charge screening. This effect could result in decreased enzyme encapsulation in the coacervate phase and therefore an increase in the observed catalase fraction in the dilute phase.

Check 3. For coacervates in solution, the reaction-diffusion model predicts the following rate constant for peroxide decomposition and pH increase

$$k_{\text{obs}}^{\text{coacervates in solution}} = k_{\text{obs}} \left[f + (1 - f) \left(\frac{1}{\alpha \tanh(3\alpha)} - \frac{1}{3\alpha^2} \right) \right] \tag{S58}$$

where $\alpha = a/a^*$ is the ratio between the coacervate droplet radius and the reaction-diffusion length. Based on the measured droplet size $a < 1$ μm and the estimated reaction-diffusion length $a^* = 6.8$ μm, the bracketed term should be close to one (> 0.99) such that $k_{\text{obs}}^{\text{coacervates in solution}}$ is indistinguishable from k_{obs}. Consistent with this expectation, a t-test between the observed t^* values for 'catalase in solution' (pooled with 'only catalase centrifuged') and 'coacervates in solution' suggests they are not significantly different (p-value $= 0.084$).

Check 4. Finally, for the isolated 'pellet' phase, the model predicts a significant reduction in the rate constant

$$k_{\text{obs}}^{\text{pellet}} = k_{\text{obs}}(1 - f) \left(\frac{1}{\alpha \tanh(3\alpha)} - \frac{1}{3\alpha^2} \right) \approx k_{\text{obs}} \frac{(1 - f)}{\alpha} \tag{S59}$$

This expression corresponds to equation (S58) but without the contribution of catalase present in solution; the second approximate expression is valid for $\alpha \gg 1$. While the observed rate constant $k_{\text{obs}}^{\text{pellet}} = 0.083 \pm 0.0063$ s^{-1} is considerably lower than $k_{\text{obs}} = 0.51 \pm 0.074$ s-1, it is not consistent with model expectations based on the pellet size which is ca. 100 times larger than the reaction-diffusion length. We attribute this discrepancy to catalase in the dilute phase that remains after removal of the supernatant and to partial redissolution of the pellet upon addition of the peroxide solution. Both of these effects would lead to an increase in the observed rate constant due to catalase present in solution—not incorporated within the coacervate pellet.
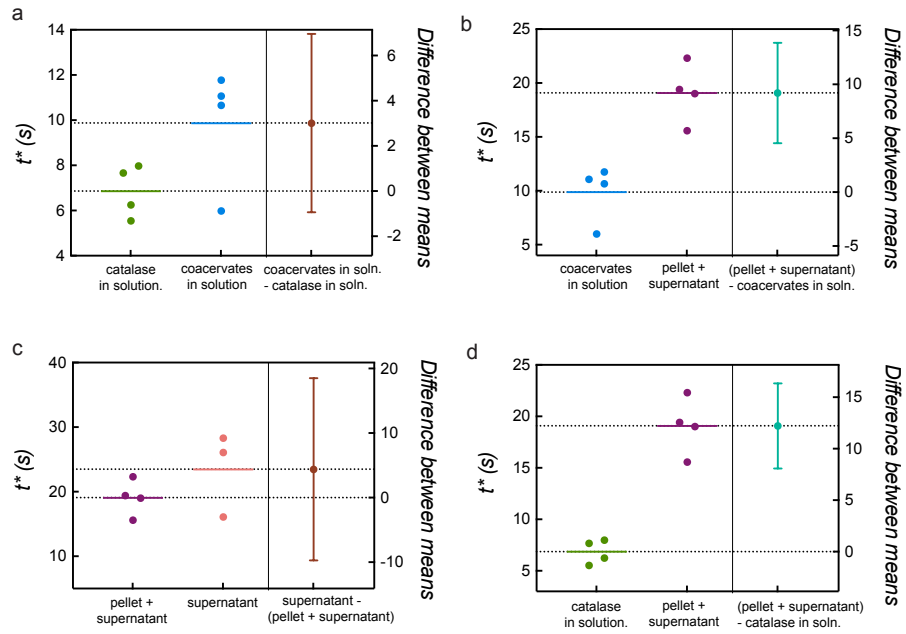
Figure S13: Estimation plots for two-tailed Welch's t-tests applied to t^* data from Table SII corresponding to experiments described in Figure 5. Each graph shows the data and mean for the two samples being compared and the effect size, or the difference between the mean t^* values. Error bars represent 95 % confidence interval for the difference in means.

7 Effects of drop coarsening on t^*

To obtain coacervates with varying size distributions, coacervate solutions of the same composition were stirred for different times while maintaining the aging time constant (time between coacervate formation and the start of the assay). Stirring does not affect the activity of the free enzyme in solution as seen by similar t^* values of just catalase in solution with (4 + 0 hr) and without stirring (0 hr) (Fig. S14, Table SIII). The area corresponding to a coacervate with a critical radius of 7 μm is 154 μm^2. The average area per microscopy image occupied by coacervates with area greater than 154 μm^2 in coacervate solutions stirred for 2 hours (2+2 hr) is 0.17 ± 0.06 mm^2 and for coacervates stirred for 4 hours (4+0 hr) is 0.27 ± 0.10 mm^2, indicating an increase in large drops as a function of time stirred. A negligible number (or area) of large drops (area > 154 μm^2) are present in unstirred coacervate solutions (0+4 hr). Therefore, this indicates that the increase in t^* as we go from unstirred coacervates in solution ($t^* = 4.7 \pm 1.6$ s) to coacervates stirred for four hours ($t^* = 8.1 \pm 2.0$ s) is due to the presence of a larger number of coacervates greater than the estimated critical size (Fig. S14, Table SIII). Experimental uncertainties in droplet size distribution do not permit quantitative analysis of t^* values based on droplet size.
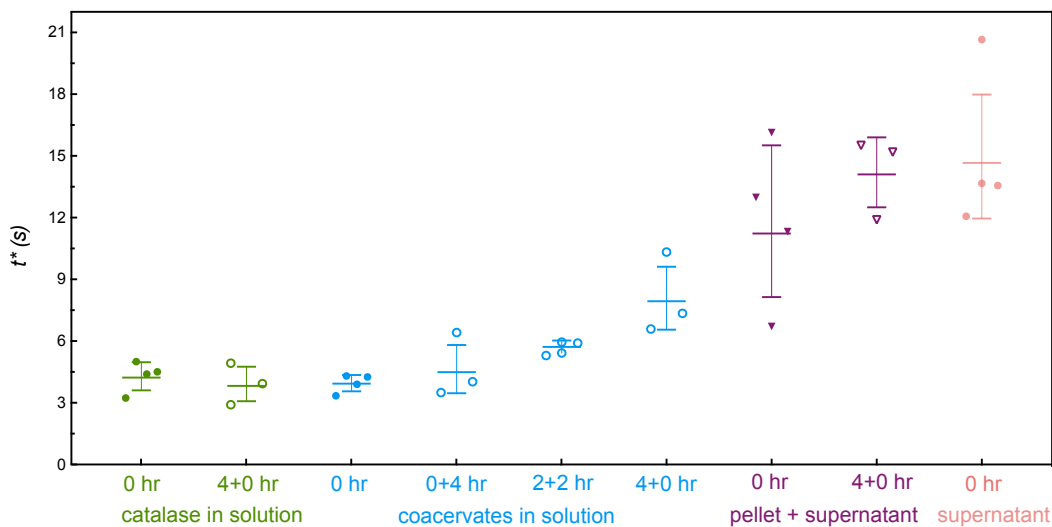

Figure S14: Comparison of t^* values obtained from pH versus time data for unaged and aged solutions. The t^* values were obtained in the same manner as for Fig. 5. The x-axis labels denote the decomposition of the total aging time into time 'stirring' + 'standing' (e.g., '4+0 hr' implies 4 hr stirring and 0 hr standing before initiating the reaction) except for the column labeled pellet+supernatant 4+0 hr. Each data point in this column was obtained by centrifuging coacervate solutions that were all aged 4 h but were stirred for different times. Catalase concentration is 0.224 mg/mL in all solutions. Mass fraction of catalase is 0.94 with the total macromolecular concentration being 0.25 mg/mL for mixed samples. Final concentration of H$_2$O$_2$ in all assays is 0.1 M.

catalase in solution		coacervates in solution				pellet+supernatant		supernatant
0 hr	4+0 hr	0 hr	0+4 hr	2+2 hr	4+0 hr	0 hr	4+0 hr	0 hr
4.40	2.91	4.26	4.03	5.91	7.35	11.32	15.53	12.08
5.00	3.93	3.35	6.41	5.96	10.33	12.98	11.89	13.67
4.51	4.93	3.90	3.50	5.31	6.59	6.72	15.19	20.66
3.24	—	4.30	—	—	—	16.13	—	13.56
4.29 ± 0.74	3.92 ± 1.0	3.95 ± 0.44	4.65 ± 1.6	5.73 ± 0.36	8.09 ± 2.0	11.8 ± 3.9	14.2 ± 2.0	15.0 ± 3.9

Table SIII: Characteristic time scales t^* for the transient pH increase in each of the experiments presented in Fig. S14. The column heading denotes the decomposition of the total aging time into time 'stirring' + 'standing' (e.g., '4+0 hr' implies 4 hr stirring and 0 hr standing before initiating the reaction) except for the column labeled pellet+supernatant 4+0 hr. Each data point in this column was obtained by centrifuging coacervate solutions that were all aged 4 h but were stirred for different times. The last row shows the arithmetic average and standard deviation for the values in each column.

Experimental details. A 2 M solution of H_2O_2 in water was prepared and the pH was adjusted to 9 using 10 M NaOH and 6 M HCl. The addition of the above H_2O_2 solution to water adjusted to pH 9 at a final concentration of 0.1 M caused a negligible increase in pH when compared to the pH increase due to the reaction. We prepared individual solutions of 0.25 mg/mL catalase and 0.25 mg/mL DEAE-dextran in water adjusted to pH 9. In a 20 mL scintillation vial, 18.8 mL of 0.25 mg/mL catalase solution was added along with 1.2 mL of 0.25 mg/mL DEAE-dextran solution to obtain coacervates at 0.94 mass fraction of catalase (total macromolecular concentration 0.25 mg/mL). The solution was mixed by vortexing for a few seconds. During a single trial, three such vials were prepared. The solution pH in each vial was re-adjusted to pH 9 after mixing. It was then capped and sealed using parafilm. The first vial was kept in an upright position for four hours (referred to as coacervates in solution 0+4 hr in Fig. S14, Table SIII). The second vial was stirred using a tube revolver rotator at a constant speed for two hours after which the vial was taken out and left upright for another two hours (referred to as coacervates in solution 2+2 hr in Fig. S14, Table SIII). The third vial was placed in the rotator at the same constant speed for four hours (referred to as coacervates in solution 4+0 hr in Fig. S14, Table SIII). As a control, a fourth vial filled with 0.25 mg/mL catalase solution was also placed in the rotator for four hours (referred to as catalase in solution 4+0 hr in Fig. S14, Table SIII). After four hours, microscopy images of the coacervate solutions in each of the vials were taken. For each vial, 100 μL of the solution was pipetted into the wells of a 96 well plate and left undisturbed for 1 minute to allow the condensed phase to settle at the bottom of the chamber. Microscopy images were taken in duplicate for each vial using two wells, and imaging was done at two different points in each well (using a lens of magnification 4X). The solution in the uncapped vial was transferred to a separate centrifuge tube. The pH of the solution in the centrifuge tube was readjusted to 9 using 0.1 M NaOH. The 2 M H_2O_2 solution was then added to the solution in the centrifuge tube at pH 9 at a final concentration of 0.1 M. The solution pH was measured every second until the pH stabilized. The characteristic time scale for each reaction (t^*) was obtained in a similar manner as mentioned previously (see Fig. 2). 18.8 mL of the catalase solution in the fourth vial was mixed with 1.2 ml of water in a centrifuge tube. The pH was re-adjusted to 9 and the reaction was carried out in the same way as

mentioned above. Each trial consisted of four reactions in total (e.g. coacervates in solution 0+4, 2+2, 4+0 hr, and catalase in solution 0+4 hr) and three such trials were done.

For the column referred to as pellet+supernatant 4+0 hr in Fig. S14, Table SIII, three vials containing coacervate solutions were prepared. Each vial was subjected to a different stirring time (0 hr, 2+2 hr, 4+0 hr) as described above, i.e., the first vial was left standing in a upright position for four hours, the second vial was placed in the rotator for two hours and then left standing for another two hours while the third vial was placed in the rotator for four hours. After four hours, the solution in each of the three vials was pipetted into a separate centrifuge tube. The pH of the solution in each centrifuge tube was readjusted to 9 followed by centrifugation at 4000 rpm at room temperature for 30 minutes to obtain a macro-scale coacervate pellet at the bottom of each tube. While each of these solutions were stirred for different times, they were all aged 4 h and then a macroscopic sized droplet was obtained by subsequent centrifugation; these three vials are included as pellet+supernatant 4+0 hr. After centrifugation, the solution pH was readjusted to 9 followed by addition of H_2O_2 in a similar manner as described above.

All assays were done in the absence of stirring. Experiments were done using a fresh batch of catalase (Sigma Aldrich C9322). Unaged solutions namely catalase in solution 0 hr, coacervates in solution 0 hr, pellet+supernatant 0 hr and supernatant 0 hr in Fig. S14, Table SIII were prepared in the same manner as Figure 5 (see Methods) using the new batch of catalase.

The area of the coacervates in the images was measured using ImageJ. The images were thresholded by conversion to a binary image wherein the condensed phase was separated from the background. Smoothing of the image was done using the Gaussian blur filter (σ: 2 pixels). The images were again converted into binary images, and the area of the thresholded coacervate phase was calculated using the *Analyze Particles* function. For each of the two sets of stirred coacervate solutions (referred to as coacervates in solution 2+2 hr and coacervates in solution 4+0 hr in Fig. S14, Table SIII), a minimum of 9 images were analyzed. For the unstirred coacervate solutions (coacervates in solution 0+4 hr in Fig. S14, Table SIII), there was a negligible amount of condensed phase visible using the above microscopy technique.

The area corresponding to a coacervate with a critical radius of 7 μm is 154 μm^2. The area of the smallest coacervates visible in the microscopy images is less than 100 μm^2 with a number of coacervates having an area greater than 500 μm^2 in each image.

Activity of free enzyme in solution remains the same after stirring as seen by similiar t^* values of catalase in solution with (4+0 hr) and without (0 hr) stirring in Fig. S14, Table SIII. The average area per microscopy image occupied by coacervates with area greater than 154 μm^2 in coacervate solutions rotated for 2 hours (2+2 hr) is 0.17 ± 0.06 mm^2 and for coacervates stirred for 4 hours (4+0 hr) is 0.27 ± 0.10 mm^2. Therefore, we estimate that a larger fraction of the total catalase present in the coacervate solutions rotated for four hours is contained within coacervates of radius $a >> a^*$ as compared to coacervates rotated for two hours. A negligible number of large coacervates present in solutions left upright suggests that almost all the enzyme present in these solutions is within drops of radius $a << a^*$. Based on this, we should see a decreasing rate of pH increase and corresponding larger t^* values as we go from unstirred to stirred coacervate solutions as more and more enzyme contained within coacervates larger than the critical size experiences a

diffusion limited reaction (the overall concentration of catalase and composition of the coacervates remain the same in all the three solutions). As expected, we see this trend in Fig. S14 and Table SIII indicating diffusion limitations in the presence of coacervates with sizes larger than the critical radius.

The methodology followed to measure the area of the condensed phase is biased towards larger coacervates as coacervates that are a few microns in size will not be detected using the above technique. Therefore, the relative contribution by coacervates much smaller than the critical size towards the catalytic reaction is unknown. Experimental uncertainties in measuring the coacervate size distributions makes it difficult to quantify the expected change in the effective rate constant for H_2O_2 consumption and hence the rate of pH increase for these aged and rotated coacervate solutions.

8   Challenges in visualizing local pH changes with indicator dyes

The reaction-diffusion model predicts transient pH differences between the inside and outside of large drops with radius $a \gg a^*$ (Fig. 6). We attempted to visualize such differences using pH indicator dyes; however, these efforts were confounded by spectral shifts in dye absorption in the presence of the enzyme and/or polymer. Here, we describe experiments to visualize reaction-induced pH changes using α-naphtholbenzein and phenolphthalein indicator dyes, which exhibit significant color differences between pH 9 and 10.

8.1 α-Naphtholbenzein

The indicator dye α-naphtholbenzein changes color from orange to green to blue as the pH is increased from 8.5 to 10.5 (Fig. S15a). Addition of 0.5 mg/mL catalase to the buffered dye solution caused a visible change in the solution color indicating a spectral shift in the dye's absorption band for the desired pH values 9.5 and 10 (Fig. S15b). This effect was further exacerbated within the catalase/DEAE-Dextran coacervate. Upon addition of H_2O_2 fuel, the solution pH increased from 9 to 10 resulting in a color change from orange/brown to green/blue in the supernatant (Fig. S15c). By contrast, the color of the coacervate material sedimented at the bottom of the vial remained brown. These results suggest that this indicator dye is too sensitive to the presence of catalase and DEAE-Dextran to make reliable estimates of the local pH within the coacervate.

Experimental Details.   A stock solution of 1 mg/mL α-Naphtholbenzein (Sigma Aldrich, 70480) in ethanol was diluted to 0.02 mg/mL α-naphtholbenzein in 10 mM sodium carbonate-bicarbonate buffers at pH from 8.5 to 10.5 (Fig. S15a).

Individual solutions of 0.5 mg/mL catalase and 0.5 mg/mL DEAE-dextran in water, each containing α-naphtholbenzein dye at a concentration of 0.02 mg/mL were prepared. The color of 0.5 mg/mL catalase in water containing 0.02 mg/mL α-naphtholbenzein at a certain pH was compared to the color of just water containing 0.02 mg/mL α-naphtholbenzein at the same pH (Fig. S15b). We mixed 14.1 mL of the 0.5 mg/mL catalase solution with 0.9 mL of the 0.5 mg/mL DEAE-dextran solution in glass vials to obtain coacervates at 0.94 mass fraction of catalase at pH 9 (at 0.02 mg/mL α-naphtholbenzein dye concentration). One of the two vials containing the coacervate solution was treated with Sigmacote to prevent an upward flow of large coacervates towards the air-water interface during the reaction. The solutions were left overnight at 4 °C to obtain a large coacervate in the form of a sedimented dense phase at the bottom of the glass vial (Fig. S15c).

The pH of a 2 M H_2O_2 solution in water was adjusted to 9 using 10 N NaOH. 0.75 mL of the 2 M H_2O_2 solution was added to the 15 mL sedimented solution in glass vials such that the final concentration of H_2O_2 was 0.1 M. The reaction caused the pH of the solution to change from 9 to 10 (Fig. S15c).
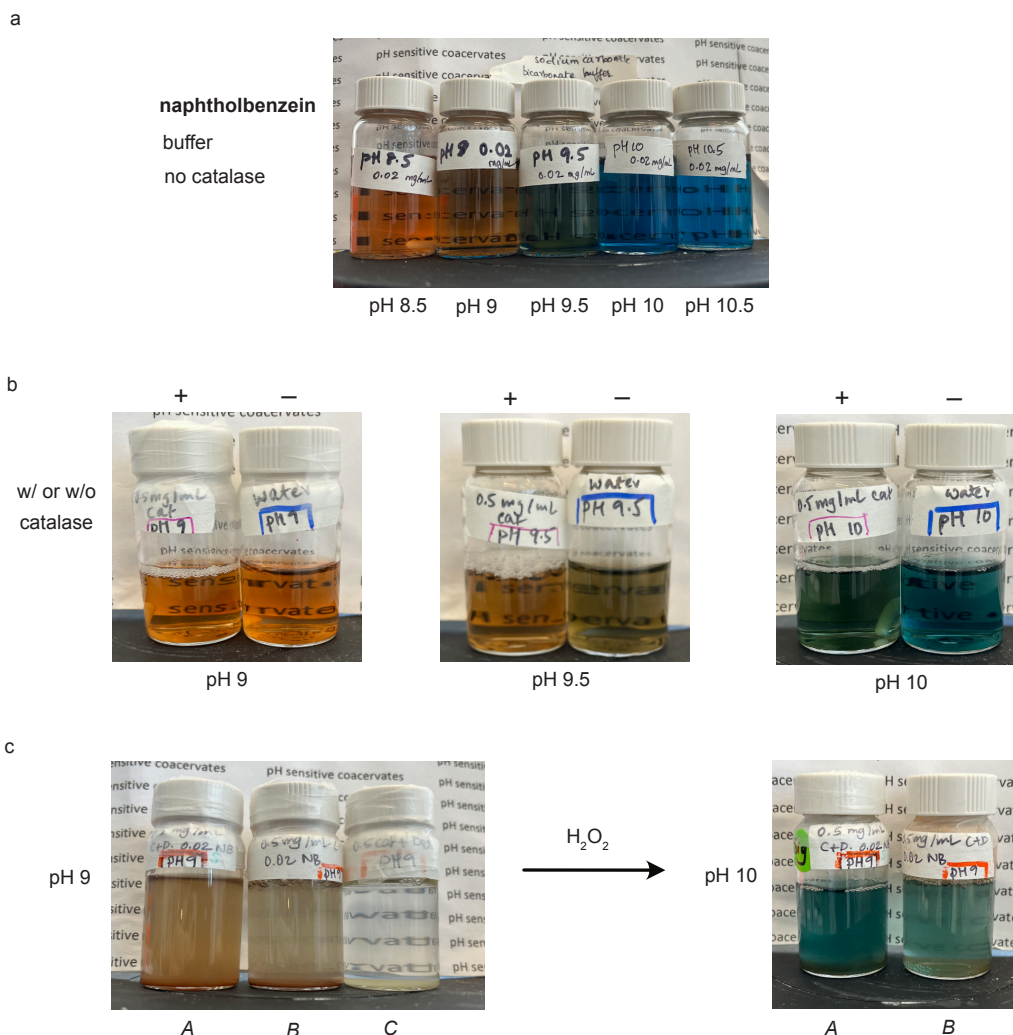
Figure S15: (a) 10 mM sodium carbonate-bicarbonate buffer with 0.02 mg/mL α-naptholbenzein at pH 8.5, 9, 9.5, 10 and 10.5. (b) α-naptholbenzein solutions with (left) and without (right) 0.5 mg/mL catalase at pH 9, 9.5, and 10. The dye exhibits a spectral shift in the presence of enzyme at pH 9.5 and 10. (c) Dispersions of catalase/DEAE-Dextran coacervates sedimented overnight at 4°C at pH 9. Solutions A and B contain 0.02 α-naphtholbenzein; solution C has no indicator dye. Solution A is prepared in a glass vial treated with Sigmacote; solutions B and C are in untreated vials. Addition of 100 mM H_2O_2 causes a reaction-induced pH increase to 10 (right). While the supernatant changes color from orange/brown to green/blue, the sedimented coacervate remains brown.

8.2 Phenolphthalein

indicator dye is colorless at pH 8 and becomes dark pink at pH 10 (Fig. S16a). The addition of 1 mg/mL catalase to the buffered dye solution caused a visible change in the solution color at pH 9 (Fig. S16b). Like α-naphtholbenzein above, experiments using this dye indicate that the enzyme alters its absorption thereby preventing reliable measurement of the pH inside the coacervate.
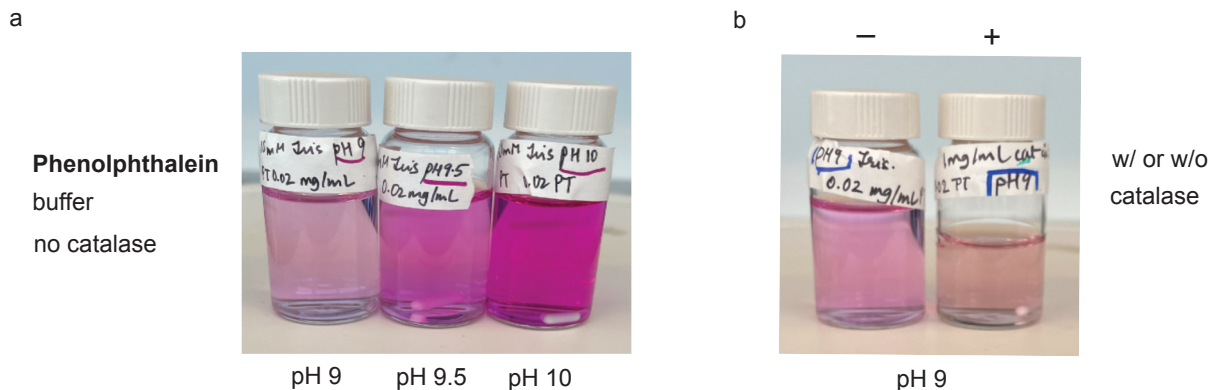

Figure S16: (a) 10 mM Tris solutions with 0.02 mg/mL phenolphthalein at pH 9, 9.5 and 10. (b) Phenolphthalein solutions with (right) and without (left) 1 mg/mL catalase at pH 9. The presence of the enzyme alters the color of the indicator solution at pH 9.

Experimental Details. A stock solution of 4 mg/mL of phenolphthalein (Sigma Aldrich, 105945) in ethanol was diluted to 0.02 mg/mL phenolphthalein in 10 mM Tris buffers at pH from 9 to 10 (Fig. S16a).

The color of 1 mg/mL catalase in 10 mM Tris buffer at pH 9 with 0.02 mg/mL phenolphthalein was compared to the color of just 10 mM Tris buffer containing 0.02 mg/mL phenolphthalein at the same pH (Fig. S16b)

References

1. Ogura, Y. Catalase activity at high concentration of hydrogen peroxide. *Arch. Biochem. Biophys.* **57,** 288–300 (1955).

2. Beers, R. F. & Sizer, I. W. A spectrophotometric method for measuring the breakdown of hydrogen peroxide by catalase. *J. Biol. Chem.* **195,** 133–140 (1952).

3. Stillinger, F. H. Proton transfer reactions and kinetics in water. *Theor. Chem. Adv.* **3,** 177–234 (1978).

4. Cummings, C. S. & Obermeyer, A. C. Phase separation behavior of supercharged proteins and polyelectrolytes. *Biochemistry* **57,** 314–323 (2018).

5. Zervoudis, N. A. & Obermeyer, A. C. The effects of protein charge patterning on complex coacervation. *Soft Matter* **17,** 6637–6645 (2021).

6. Frankel, E. A., Bevilacqua, P. C. & Keating, C. D. Polyamine/nucleotide coacervates provide strong compartmentalization of Mg^{2+}, nucleotides, and RNA. *Langmuir* **32,** 2041–2049 (2016).

7. Alptekin, O., Tükel, S. S., Yıldırım, D. & Alagöz, D. Immobilization of catalase onto Eupergit C and its characterization. *J. Mol. Catal. B Enzym.* **64,** 177–183 (2010).

8. Lardinois, O. M., Mestdagh, M. M. & Rouxhet, P. G. Reversible inhibition and irreversible inactivation of catalase in presence of hydrogen peroxide. *Biochim. Biophys. Acta, Protein Struct. Mol. Enzymol.* **1295,** 222–238 (1996).

9. *Handbook of Chemistry and Physics* 72nd ed. (ed Lide, D. R.) (CRC Press, Boca Raton, Florida, 1991).

10. Karoui, H., Seck, M. J. & Martin, N. Self-programmed enzyme phase separation and multi-phase coacervate droplet organization. *Chem. Sci.* **12,** 2794–2802 (2021).